# Properties of a large-scale flux rope and current sheet region on the dayside of Mars: MGS MAG/ER and MEX ASPERA-3 ELS observations

Yasir I.J. Soobiah [a,*], James A. Wild [a], Mathew J. Beharrell [a], Stas Barabash [b], Robert J. Lillis [c], David L. Mitchell [c], Andrew J. Coates [d], J. David Winningham [e], Rudy A. Frahm [e]

[a] Department of Physics, Lancaster University, Lancaster, UK
[b] Swedish Institute of Space Physics, Institutet för rymdfysik (IRF), Kiruna, Sweden
[c] Space Sciences Laboratory, University of California Berkeley, Berkeley, CA, USA
[d] Mullard Space Science Laboratory, University College London, Holmbury St. Mary, Dorking, Surrey, UK
[e] Southwest Research Institute, San Antonio, TX, USA

## ARTICLE INFO

## ABSTRACT

We present dual spacecraft observations by MGS MAG/ER and MEX ASPERA-3 ELS of a large-scale magnetic flux rope on the dayside of Mars that occurs in close proximity to the crustal magnetic fields and a dayside current sheet region. A current sheet (including the large-scale flux rope) was observed on repeated MGS orbits when the draped solar wind magnetic field present in the ionosphere had a $+B_y$ component (in MSO). Minimum Variance Analysis (MVA) of the large-scale flux rope and two current sheet crossings that occur after show a common peak in magnetic field along the intermediate variance direction, indicating the normal component of a reconnecting current sheet. All repeated orbits demonstrated evidence of a plasma boundary by the decrease in electron differential flux above 100 eV when moving into regions dominated by the crustal magnetic field, and coincided with the measured magnetic field strength being double the undisturbed crustal magnetic field. We argue this forms evidence of magnetic reconnection between crustal magnetic fields and draped solar wind magnetic field (from ionosphere or magnetosheath) at a "mini-magnetopause" type boundary on the dayside of Mars. Similar electron pitch angle distributions observed during the large-scale flux rope, current sheet crossings, and regions of radial crustal magnetic field, suggest these regions share a common magnetic field topology for the trapping of magnetosheath particles on open crustal magnetic fields on the dayside of Mars. As such, indicates a trapping quadrupole magnetic field exist either at the magnetic reconnection X-line region or where open crustal magnetic fields meet oppositely directed solar wind magnetic field. At a time when the draped solar wind magnetic field present in the ionosphere was weaker in strength, the current sheet crossing was observed over an extended region of 2000 km. The extended current sheet demonstrated properties of a hot diamagnetic region and features of a mirror mode structure or magnetic hole, the first time such a structure has been found in the ionosphere of Mars. Observations suggests lower energy electrons could be accelerated by a local process of perpendicular heating/pitch angle diffusion and supports similar results at the Earth's polar cusp reported by Nykyri et al. (Nykyri et al. [2012]. J. Atmos. Sol-Terr. Phys. 87, 70). Such large scale and energetic structures are usually associated with regions beyond a planet's ionosphere, and the occurrence within the ionosphere of Mars may have an important impact on escape processes and the evolution of the martian atmosphere.

## 1. Introduction

The dayside ionosphere of Mars in regions away from crustal magnetic fields are characterised by the magnetic field topology of draped solar wind magnetic fields (Brain et al., 2007). This indicates that these regions of the martian ionosphere are usually penetrated and magnetised by the solar wind magnetic field. However, when the dynamic pressure of the solar wind is low enough it is possible for the thermal pressure of the martian ionosphere to exclude the solar wind more effectively and remain unmagnetised by the solar wind magnetic field. This is more often the case at Venus due to its thicker atmosphere (Russell, 1990). During such conditions, shear-related instabilities between the shocked solar wind plasma and the ionosphere can lead to solar wind magnetic

* Corresponding author.

field entering the ionosphere in the form of small filamentary structures of twisted magnetic field, or magnetic flux ropes (Vignes et al., 2004; Elphic and Russell, 1983). A magnetic flux rope is typically defined as a wrapping of magnetic field lines around a strong core magnetic field along the central axis (Russell and Elphic, 1979). Filamentary flux ropes observed in the dayside ionosphere of Mars and Venus are characterised by magnetic field similar in strength to that of the draped solar wind (10's nT) and a small radial size (10's km).

When the ionosphere of Mars and Venus is magnetised by draped solar wind magnetic field, flux rope signatures occur with larger magnetic field enhancements (100's nT) and radial size (100's km) (Brain et al., 2010; Zhang et al., 2012b). The large-scale flux ropes have primarily been studied at the terminator of Mars (Brain et al., 2010; Morgan et al., 2011; Beharrell and Wild, 2012) and Venus (Zhang et al., 2012b), where there is a greater occurrence (Beharrell and Wild, 2012). Large-scale flux ropes that occur near the terminator of Mars have been identified downstream from the strong martian crustal magnetic fields in the southern hemisphere, suggesting regions of closed crustal magnetic field are stretched downstream by the solar wind flow forming a plasmoid-like structure (Brain et al., 2010; Morgan et al., 2011; Beharrell and Wild, 2012). Morgan et al. (2011) presented dual spacecraft observations at the Mars terminator of a large-scale flux rope that was quasi-steady between each spacecraft pass of 30 min. Beharrell and Wild (2012) showed these structures are also quasi-stationary over approximately 7 days or more when observed on successive orbits of the Mars Global Surveyor (MGS) spacecraft that repeat the same path in Mars planetocentric (MPC) and Mars Solar Orbital (MSO) reference frames. Brain et al. (2010) proposed that observations of current sheets between the large-scale flux ropes and the upstream crustal magnetic field region, was indicative of magnetic reconnection and the detachment of the plasmoid, causing a bulk removal process of the ionosphere.

Zhang et al. (2012b) has shown that large-scale flux ropes of a similar magnetic field strength and radial size to those observed at the Mars terminator also occur near the terminator of Venus. The observations of large-scale flux ropes at Venus raises a number of questions (Zhang et al., 2012b), for example if a process common to both Mars and Venus is responsible for the signatures of large-scale flux ropes without the involvement of the crustal magnetic fields, or if perhaps the venusian crust is capable of supporting remanent magnetic fields despite the high surface temperature being comparable to the Curie temperature?

Flux ropes signatures have also been observed beyond the terminator within the induced magnetotail of Mars (Eastwood et al., 2008, 2012) and Venus (Slavin et al., 2009; Zhang et al., 2012a). The flux ropes of the magnetotail of Mars and Venus are found to take place in-between crossings of the central current sheet that separate oppositely orientated magnetic field of the magnetotail, and have been related to magnetic reconnection (Eastwood et al., 2008; Zhang et al., 2012a). Flux ropes of the Mars magnetotail are characterised by similar weak magnetic field strength and radial size as filamentary ionospheric flux ropes (Eastwood et al., 2008, 2012), whereas flux ropes from the Venus magnetotail have been observed with larger sizes (1000's km) (Slavin et al., 2009; Zhang et al., 2012a).

There is also evidence large-scale flux ropes can occur on the dayside ionosphere of Mars, where in a region of only weak crustal magnetic field at ~50° SZA, Morgan et al. (2011) showed measurements by the Mars Express (MEX) MARSIS Radio Sounder instrument of a localised region of strongly enhanced magnetic field. A statistical study by Briggs et al. (2011) reported that several of the strongest flux ropes (exceeding 80 nT) observed on the dayside of Mars as associated with crustal magnetic fields.

Since current sheet crossings observed on the dayside of Mars are found to cluster around the perimeters of strongly magnetised crustal magnetic field and with smaller than expected rotations in the IMF draping, suggest regions of strongly magnetised crust on Mars also have an indirect role in the formation of current sheets in the dayside ionosphere (Halekas and Brain, 2010). This could indicate a possible association between the formation of large-scale flux ropes on the dayside of Mars with current sheet crossings, as observed with flux ropes of the magnetotail of Mars and Venus. Indeed, magnetic reconnection on the dayside of Mars between crustal and solar wind sources is likely to drive changes in magnetic topology (Brain, 2006b) and therefore, may also relate to the properties of current sheets and flux ropes observed on the dayside of Mars.

A possible cause for such a process to occur at the perimeter of strong crustal magnetic field regions, could be the presence of a "mini-magnetopause" type boundary separating regions dominated by crustal magnetic field from surrounding regions of plasma. A magnetopause will support the formation of a current sheet due to the magnetic field gradient that occurs between the different regions of plasma separated by the magnetopause. Magnetic flux ropes will also be able to form at a magnetopause when conditions allow for magnetic reconnection and a connection is created between the different regions of plasma separated by the magnetopause.

Until now, observations have been lacking confirming the presence of a mini-magnetopause boundary around the crustal magnetic fields of Mars. It is unknown if the crustal magnetic fields have sufficient magnetic field pressure for the formation of a mini-magnetopause. Also, the large ion gyroradius size present in the martian ionosphere in relation to the scale-size of the crustal magnetic fields, would suggest conditions for the formation of a magnetopause under the ideal magnetohydrodynamics (MHD) regime may not be satisfied. However, non-ideal MHD simulations of the solar wind interaction with Mars and its strong crustal magnetic fields by Harnett and Winglee (2003) demonstrated that the strong crustal magnetic fields could form a magnetopause-like structure (i.e., a mini-magnetopause) in place of an MPB when located on the dayside and facing the solar wind.

In this paper we present dual spacecraft observations by MGS Magnetometer/Electron Reflectometer (MAG/ER) and MEX Analyzer of Space Plasmas and Energetic Atoms-3 (ASPERA-3) Electron Spectrometer (ELS) of a large-scale flux rope observed on the dayside of Mars in-between a reversal of magnetic field directions and in close proximity to the crustal magnetic fields. We also present MAG/ER observations from consecutive MGS orbits repeating the same path through the location of the large-scale flux rope. The repeated MGS orbits reveals a plasma boundary from the measurement of electrons as MGS exits regions dominated by crustal magnetic fields and on occasions a $+B_y$ component is measured in the draped solar wind magnetic field that has advected into the ionosphere, a dayside current sheet is detected near the location where the large-scale flux rope was observed.

## 2. Instrumentation

This analysis includes a comparison of the work initiated by Beharrell and Wild (2012) for MGS data with observations made by MEX. Beharrell and Wild (2012) searched for the magnetic signatures of flux ropes in MGS Magnetometer (MAG) data during the mapping phase of MGS from March, 1999 to November, 2006. During mapping phase, MGS has a Sun-synchronous orbit near 2:00 am/2:00 pm, with an altitude ranging from 368 km to 438 km. The orbit of MGS also retraces its path in the Mars

planetocentric frame (MPC) after 88 orbits (7 martian solar days), with a small offset to the east of 58.6 km when measured at the equator.

The MGS MAG instrument (Acuña et al., 1999) provided three-dimensional magnetic field measurements and we present measurements at 0.75 s resolution (dropping to 1.5 s or 3 s, depending on telemetry allocation). The MGS Electron Reflectometer (ER) instrument (Mitchell et al., 2001) was a symmetric hemispherical top-hat electrostatic analyser and measured electrons in the energy range of 10 eV to 20 keV with an energy resolution of $\Delta E/E = 0.25$. We present ER data at a time resolution of 2 s, 4 s, or 8 s resolution, containing a sweep of 19 energy channels. Since MGS is a three-axis stabilized spacecraft, electron pitch angle data is limited by the ER field of view of $14° \times 360°$, which is divided into 16 sectors of 22.5° wide.

We also present data from MEX ASPERA-3 instrument (Barabash et al., 2004), which includes an Electron Spectrometer (ELS) and Ion Mass Spectrometer (IMA). ELS is a compact spherical top-hat electrostatic analyser and collimator system, and measures electrons in the energy range of 1 eV to 20 keV with an energy resolution of $\Delta E/E = 0.08$. The time resolution for ELS is 4 s to make a sweep of 128 energy levels. The intrinsic field of view for ELS is $4° \times 360°$ and is divided into 16 sectors of 22.5° wide. IMA measures ions of energies 0.01–40 keV/q for the main ion components $H^+$, $H_2^+$, $He^+$ and $O^+$, and the group of molecular ions (20–80 amu/q). However, an energy table used by IMA before May 2007 did not adequately resolve ion measurements below 50 eV and as a result had difficulty in detecting ions of planetary origin.

MEX has a highly inclined orbit with an apoapsis of nearly 10,000 km and periapsis of nearly 300 km with an orbital period of 6.7 h. The orbit of MEX also retraces its path in MPC after 11 orbits (3 martian solar days).

## 3. Observations

To arrive at a list of possible flux rope signatures, Beharrell and Wild (2012) used a sliding median function on a timescale of around 1–2 min to search MAG data for deviations in the magnetic field from the crustal magnetic field with a similar window size (see Beharrell and Wild (2012) for further details). Using this method, 21,885 enhancements in the magnetic field measurements were identified during the mapping phase of MGS between March, 1999 and November, 2006. From these signatures, 85 were found to occur near a conjunction of the MEX spacecraft to within 500 km and 40 min of MGS MAG measuring the enhancement. Data was available from ASPERA-3 ELS for 53 of the 85 MGS-MEX conjunctions. A minimum variance analysis (Sonnerup and Scheible, 1998) of these 53 events showed that 29 involved rotations of the magnetic field vector as would occur during an encounter of a magnetic flux rope.

### 3.1. Large-scale flux rope on the dayside of Mars: MGS MAG/ER observations

Fig. 1a–c shows the orbit configuration in Mars Solar Orbital frame (MSO) of MGS (blue) and MEX (black) on 21st July, 2006, ($82° L_S$), when MGS MAG observed a large-scale magnetic flux rope at 23:37:46 UT (indicated by the red segment). Fig. 1d shows the orbit paths in latitude and east longitude of MGS (square symbols) and MEX (cross symbols) over a map of the radial component of crustal magnetic field as measured by MGS. Fig. 1e shows the range in km of the MEX spacecraft from the location MGS observed the large-scale flux rope signature.

Fig. 2a and b shows 16 min of magnetic field measurements by MAG as the orbit of MGS progressed northwards. Fig. 2a compares

the magnetic field strength measured by MAG (black) to the Cain model of the crustal magnetic field (red) (Cain et al., 2003) and shows that as MGS exits a region of strong crustal magnetic field to the south, the MAG instrument observes a large amplitude enhancement in the magnetic field at the edge of this region from 23:36:55 UT to 23:41:41 UT. The magnetic field strength reaches a peak of around 130 nT at 23:37:46 UT. Note, that the magnetic field enhancement takes place near 0° latitude where the Cain model shows a weak region of crustal magnetic field (around 30 nT) with a negative radial component. Morgan et al. (2011), reported a similar observation by MARSIS of a strong localised enhancement in magnetic field strength over a weak region of crustal magnetic field that occurred at the northward edge of stronger magnetised crust further south.

Alongside observing a large amplitude enhancement in the magnetic field strength, MAG also measures rotations in the magnetic field vectors highlighted by a well-defined bi-polar variation in the $B_x$ component, as would suggest the presence of a flux rope (Russell and Elphic, 1979). A rotation in $B_y$ is also observed from $-B_y$ before the flux rope to $+B_y$ afterwards and indicates the flux rope is observed during a current sheet crossing.

The result of a minimum variance analysis between 23:39:35 UT and 23:41:41 UT is presented in Fig. 4, which shows the magnetic field hodograms of the large-scale flux rope signature. We have used the same convention for defining the coordinate system of the flux rope as Beharrell and Wild (2012), where the minimum variance direction, $n$, is aligned with the flux rope axis, the corresponding maximum variance direction is $l$, and $m$ completes the orthogonal set. Fig. 4 shows an approximately circular polarization in the plane containing the maximum and intermediate variance ($l - m$ plane), while in the planes containing $l - n$ and $m - n$ there is a small out of plane bend indicated by a negative axial field, also marking the interior of the flux rope (coloured in blue). Note, the magnetic field in the minimum variance direction, $n$, is mostly negative and of the same sign, compared to the other directions that show both positive and negative magnetic field. This supports the flux rope axis as most likely along the minimum variance direction.

The MVA analysis of Fig. 4 provided direction eigenvectors for the maximum variance of $l = (0.13, -0.98, 0.11)$ (approximately aligned along $-Y$ in MSO), the intermediate variance of $m = (0.99, 0.12, -0.09)$ (approximately aligned along $+X$ in MSO) and the minimum variance of $n = (0.08, 0.12, 0.99)$ (approximately aligned along $+Z$ in MSO). The MVA analysis gave eigenvalues of 3822.5 for the maximum variance, 1692.5 for the intermediate variance and 52.8 for the minimum variance. Therefore, the large-scale flux rope has an intermediate/minimum variance eigenvalue ratio equal to 32 and maximum/intermediate variance eigenvalue ratio equal to ~2.

In addition to the main rotation of the magnetic field vectors are perturbations in the magnetic field within the flux rope at around 23:36:30 UT, 23:38:45 UT and 23:39:40 UT. The largest perturbation at 23:36:30 UT occurs as MAG starts to measure the complete departure of all magnetic field vectors from the Cain model of the crustal magnetic field. This sudden rotation in magnetic field indicates the presence of a current sheet separating the regions of magnetic field from the flux rope and strong crustal magnetic fields. The smaller perturbations show deflections in the magnetic field direction similar to that caused by field aligned currents that occur when peaked or auroral-type electron distributions are detected in the nightside of Mars (Brain et al., 2006a).

ER data of electrons for the same period is presented in Fig. 2d and e showing the energy-time spectrogram (in units of differential flux $(cm^2\ sr\ s\ eV)^{-1}$) and pitch angle distribution (binned between 10–50 eV, 50–100 eV, 100–500 eV and 500–1000 eV respectively). The pitch angle distribution is normalised to the
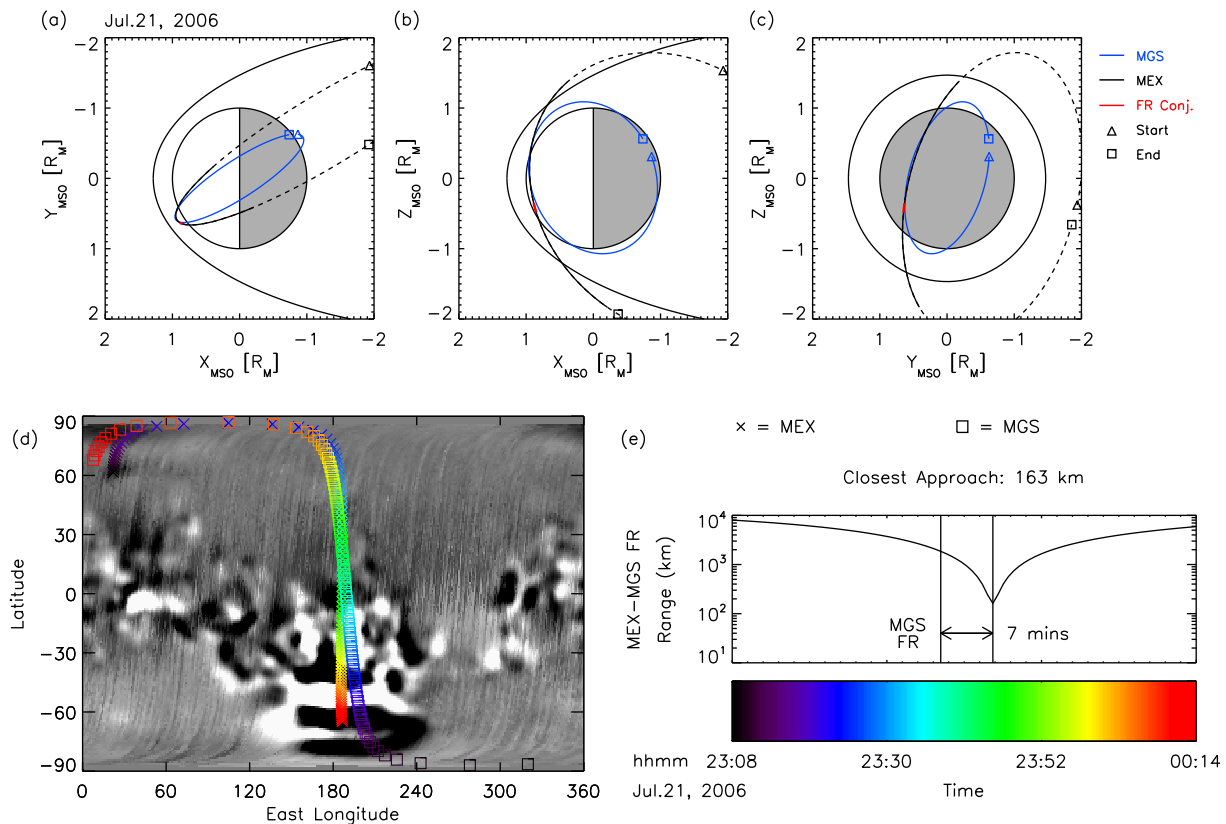
**Fig. 1.** Orbit geometry for Mars Global Surveyor and Mars Express during a conjunction on the 21st July 2006. (a–c) Displays the MSO position for MGS in blue, MEX in black and the location of a large amplitude enhancement in magnetic field in red. A triangle and square symbol denotes the start and end of each orbit respectively. (d) Orbit paths of MGS denoted by squares and MEX by × in rectangular planetary coordinates and coloured according to time (bottom right). (e) Range of MEX from the location of a large amplitude enhancement in magnetic field as measured by MGS MAG. (For interpretation of the references to colour in this figure legend, the reader is referred to the web version of this article.)

average flux over all pitch angles for each energy and time bin. The cyan bar on the top of Fig. 2d highlights the regions of ionospheric electrons that ER observed before and after large-scale flux rope. The region of ionosphere measured from 23:43:50 UT to 23:45:45 UT is characterised by magnetic field of nearly constant orientation and magnetic field strength of ~40 nT. This demonstrates the magnetic field of the ionosphere surrounding the southern crustal magnetic fields is ordered and of enhanced magnetic field strength, as is usually the case when the piled-up magnetic field from the draped solar wind magnetic field has entered the ionosphere. At times of low dynamic pressure of the solar wind, the thermal pressure of the martian ionosphere will be able to exclude the solar wind magnetic field more effectively. Ionosphere that is not magnetised by the solar wind is characterised by magnetic field that is typically weaker (<10 nT), more variable and involves sudden changes in magnetic field strengths and rotation from the presence of small filamentary flux ropes (Russell, 1990).

ER begins to measure a greater differential flux of electrons (red bar at the top of the panel) as MGS encounters the flux rope at around 23:36:35 UT, in particular between energies of 20 eV and 100 eV. The electron differential flux continues to increase until a peak is reached at the time the peak magnetic field strength of the flux rope is measured. Fig. 2e shows that there is unfortunately no pitch angle data available at this time. However, for the remainder of the flux rope encounter, MGS observes electrons that have a different pitch angle distribution depending on the energy measured. For energies less than 100 eV and closest to the flux rope peak magnetic field strength, the electrons are more field aligned. As MGS progress through the flux rope there is a change towards to a more trapped distribution near 90° pitch angles. For energies

greater than 100 eV, electrons demonstrate a trapped pitch angle distribution throughout the flux rope, since the normalised flux is at a maximum near 90° pitch angles.

Fig. 3 shows the pitch angle distribution function averaged between 23:38:30 UT and 23:39:25 UT, progresses from field aligned electrons at lower energies to trapped electrons at higher energies, with a slightly enhanced flux of electrons at intermediate pitch angles between 20 eV and 100 eV. This indicates a pitch angle diffusion process is taking place as MGS moves through the flux rope structure.

As MGS passes the flux rope from 23:42:10 UT to 23:43:50 UT (purple bar at the top of the panel), ER then measures a decrease in the differential flux of electrons below 30 eV similar to that observed in a plasma depletion region (Øieroset et al., 2004). Unfortunately, there is limited pitch angle coverage in this region and we are unable discuss this further.

### 3.2. Large-scale flux rope on the dayside of Mars: MEX ASPERA-3 ELS observations

The location of MGS at the time of the large-scale flux rope observation on 21st July, 2006, was subject to a conjunction with the MEX spacecraft, which Fig. 1e shows passed within 163 km 7 min later. Fig. 1a–d shows the MEX orbit path was co-aligned with that of MGS, however moving southwards instead of northwards. Fig. 5a and b presents electron energy-time spectrograms measured by the MEX ASPERA-3 ELS instrument.

The solid black line in Fig. 1a–c indicates the part of the MEX orbit that was within 30 min of closest approach to the location MGS measured the peak magnetic field strength of the flux rope
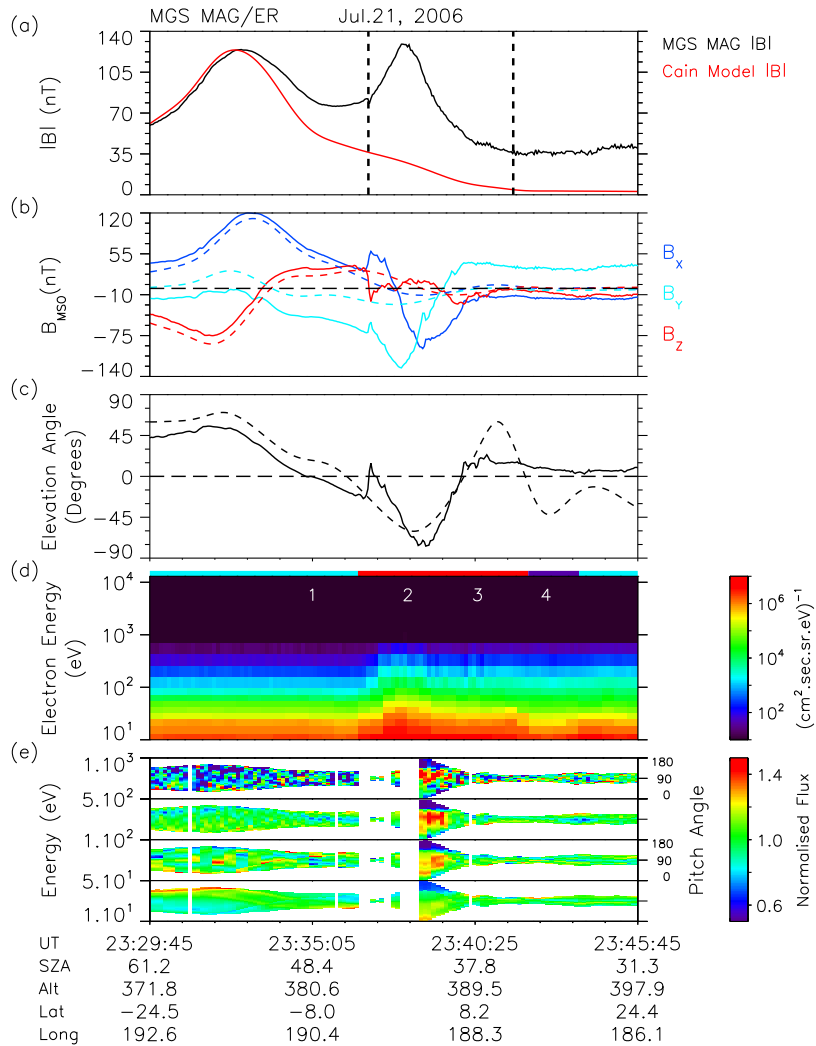
**Fig. 2.** MGS Magnetometer and Electron Reflectometer data from the dayside of Mars on 21st July 2006 and at 82° $L_s$, centred on a large amplitude enhancement in magnetic field. (a) Magnetic field strength measured by MAG (black) compared to the Cain model of the crustal magnetic field (red). Vertical dashed lines in Fig. 2a are identified for use with Fig. 4. (b) Magnetic field vectors measured by MAG and Cain model (dashed) in MSO coordinates. (c) Elevation angle of the measured (solid) and Cain model magnetic field (dashed). (d) Energy-time spectrogram of electron differential flux as measured by ER. Cyan, red and purple bars denotes regions of ionosphere, energised electrons and plasma depletion respectively. Numbers 1 to 4 identify the periods used for comparing energy spectra in Fig. 6. (e) Electron pitch angle distribution separated into four energy bins. (For interpretation of the references to colour in this figure legend, the reader is referred to the web version of this article.)
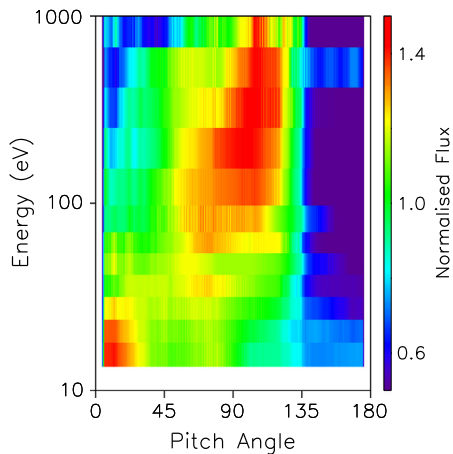


**Fig. 3.** Average electron pitch angle distribution as a function of energy between 23:38:30–23:39:25 UT on 21st July, 2006. The averaging period overlaps region of the large-scale flux rope (region 2) and its trailing edge (region 3) indicated in Fig. 2d. Pitch angle distributions at each energy are normalised.

at 23:45:25 UT and also near pericentre at 23:37:26 UT. The electron data from the ASPERA-3 ELS instrument centred on closest approach to the flux rope location measured by MGS MAG is shown in Fig. 5a after averaging over those ELS sectors that do not have the spacecraft it the field of view. We have also corrected the data for spacecraft potential using the method from Fränz et al. (2006). Note, MEX has a spacecraft charge of approximately +8 V in the magnetosheath and approximately −5 V in the ionosphere, which can prevent ELS measuring the cold component of electrons in the ionosphere. The integrated density, $n_e$ (cm$^{-3}$), from ELS is also presented in Fig. 5a and has been determined using the method from Fränz et al. (2006).

At closest approach to the flux rope location measured by MGS MAG and at the centre of Fig. 5a, ELS observes a change of plasma compared to the ionosphere measured before 23:41:04 UT and after 23:46:20 UT. At first ELS measures a depletion of plasma between 23:41:04 UT and 23:42:04 UT, when both electron density and differential flux decrease (purple bar at the top of the panel). In the region of ionosphere between 23:40:00 UT and 23:41:00 UT there was an average ELS differential flux integrated between 10 eV and 50 eV of $1.74 \times 10^7$ (cm$^2$ sr s eV)$^{-1}$ and integrated
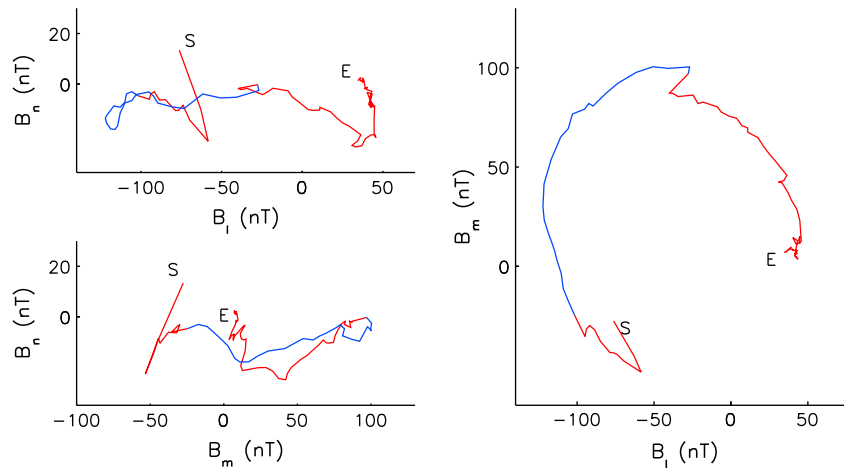
**Fig. 4.** (a–c) Hodograms for magnetic field measurements during period identified by dashed lines in Fig. 2a. Axes labelled *l* corresponds to the maximum variance direction, *m* to the intermediate and *n* to the minimum variance direction, which is also aligned with the flux rope axis. The line is coloured blue inside the flux rope and red outside. (For interpretation of the references to colour in this figure legend, the reader is referred to the web version of this article.)
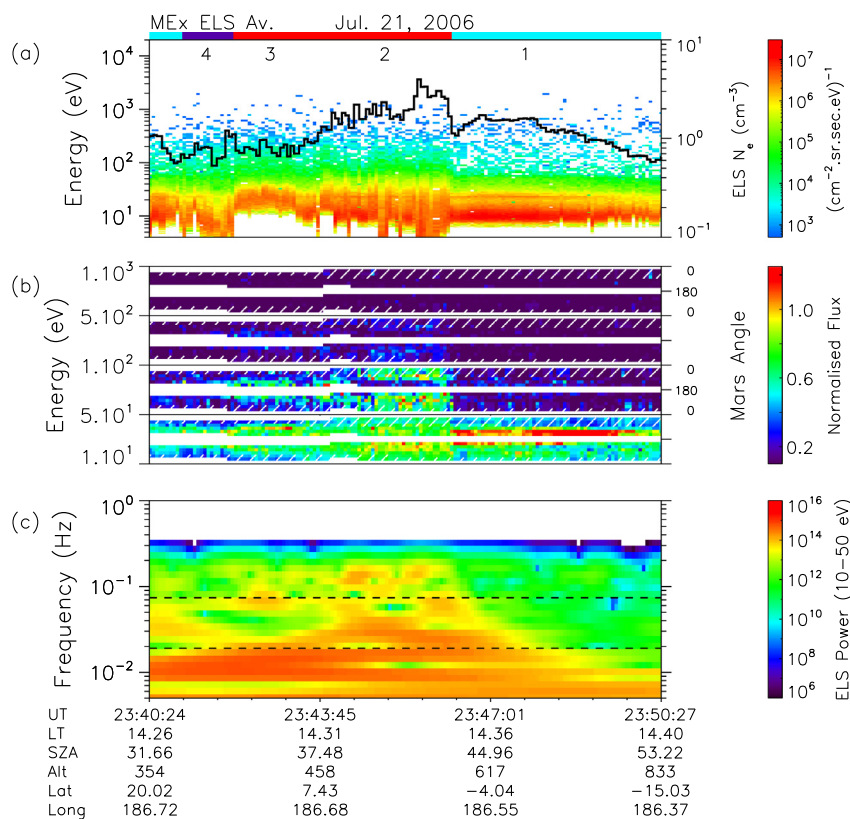


**Fig. 5.** MEX Analyzer of Space Plasmas and Energetic Atoms-3 Electron Spectrometer data during a conjunction with MGS and encounter with the location of a dayside large-scale flux rope. (a) Energy-time spectrogram of differential flux of electrons and integrated electron density ±5 min of closest approach to the location of the magnetic field enhancement measured by MGS MAG. Cyan, red and purple bars denotes regions of ionosphere, energised electrons and plasma depletion respectively. Numbers 1 to 4 identify the periods used for comparing energy spectra in Fig. 6. (b) Energy distribution function of electrons with respect to Mars nadir separated into four energy bins. Towards Mars is represented by 0° and away from Mars is represented by 180°. Areas shaded by white diagonal lines indicate parts of the distribution function that have the spacecraft in the field of view and where the data has been interpolated. (c) Wavelet transform for electron differential flux summed between 10 eV and 50 eV. Dashed lines identify periodicities between 20 mHz (∼50 s) and 70 mHz (∼14 s). (For interpretation of the references to colour in this figure legend, the reader is referred to the web version of this article.)

density of 0.96 cm$^{-3}$. This compared to $1.00 \times 10^7$ (cm$^2$ sr s eV)$^{-1}$ and 0.82 cm$^{-3}$ averaged between 23:41:04 UT and 23:42:04 UT. As MEX reaches closest approach to the flux rope location measured by MGS MAG, ELS begins to measure electrons with greater differential flux between 23:42:04 UT and 23:43:45 UT as shown by (red bar at the top of the panel), however with less integrated density

than the ionosphere observed between 23:40:00 UT and 23:41:00 UT (cyan bar at the top of the panel). In the region between 23:42:04 UT and 23:43:45 UT there was an average ELS differential flux integrated between 10 eV and 50 eV of $2.10 \times 10^7$ (cm$^2$ sr s eV)$^{-1}$ and integrated density of 0.84 cm$^{-3}$. By the time MEX is at the nearest distance to the flux rope between

23:43:45 UT and 23:46:20 UT (red bar at the top of the panel), ELS measures a further increase in the differential flux of electrons between energies of 10 eV and 50 eV. In the region between 23:43:45 UT and 23:46:20 UT there was an average ELS differential flux integrated between 10 eV and 50 eV of $2.8 \times 10^7$ ($cm^2$ sr s eV)$^{-1}$ and integrated density of 2.06 $cm^{-3}$. The electron density of this region is twice as large as the ionosphere observed between 23:40:00 UT and 23:41:00 UT. ELS then returns to measuring iono-spheric plasma after 23:46:20 UT (cyan bar at the top of the panel).

Fig. 6 compares the electron energy spectra measured by ER and ELS from the different regions when passing the location of the flux rope with energy spectra of the magnetosheath, also measured by ER (typical spectra as shown in other studies) and ELS (ELS data inbound of Fig. 5a, at 23:20:00 UT). Fig. 6 demonstrates that below 100 eV and for the main part of the distribution, ELS observes the same regions of plasma as ER when passing the flux rope but in reverse order since MEX was travelling southwards and in the opposite sense to MGS. Therefore, the plasma regions present at and around the location of the flux rope remained stationary for the 7 min between each spacecraft pass. Note, the comparison is affected above energies of 100 eV due to different instrument sensitivities of ER and ELS. Brain et al. (2006c), reported similar "cross-calibration" of ER and ELS data during a conjunction of the MGS and MEX spacecraft.

The electron energy spectra measured by both ER and ELS at the location of the flux rope is similar to that found in the magneto-sheath, although with reduced differential flux. However, the inte-grated electron density from ELS at this location is closer to the electron density from the magnetosheath just prior to the MPB (inferred from the ELS data inbound of Fig. 5a at 23:31:00 UT and

not shown). Further likeness to the magnetosheath is found by the fluctuations in the density and differential flux of electrons found when crossing the flux rope location. A wavelet analysis of the electron differential flux integrated between energies of 0 eV and 50 eV is shown in Fig. 5c (wavelets calculated using a Morlet transform with wave number 6, as suggested by Espley et al. (2004)). The wavelet analysis demonstrate there is appreciable amplitudes at periodicities from ~20 mHz (~50 s) to ~100 mHz (~10 s), ultra-low frequencies (ULF) similar to that observed in the magnetosheath prior to and after passing the location of the flux rope (at earlier and later UT than shown between 23:15:00 UT and 23:31:45 UT and between 23:53:00 UT and 00:15:00 UT and not shown). The electron oscillations maybe be driven by the similar gyrofrequency of $O^+$ ions, as is also predicted to be the case for oscillations in the differential energy flux of elec-trons (Winningham et al., 2006) and magnetic field fluctuations in the magnetosheath (Espley et al., 2005). Fig. 5a shows ELS also measures photoelectrons in the region of the large-scale flux rope (region 2) at the same energy as photoelectrons measured in the region of the crustal magnetic fields (region 1) at later UT (23:46:20 UT–23:49:40 UT). This could suggest a direct connection has been established between the shocked solar wind and crustal magnetic field regions and has allowed the two plasma popula-tions to mix.

Fig. 6c and d shows that the region corresponding to the trailing edge of the large-scale flux rope (region 3) and the region when exiting the large-scale flux rope (region 4) have similarities to the MPB and MPR inferred from the ELS data inbound of the large-scale flux rope (at earlier UT than shown at 23:31:00 UT and 23:32:00 UT respectively). This suggests that perhaps ER and
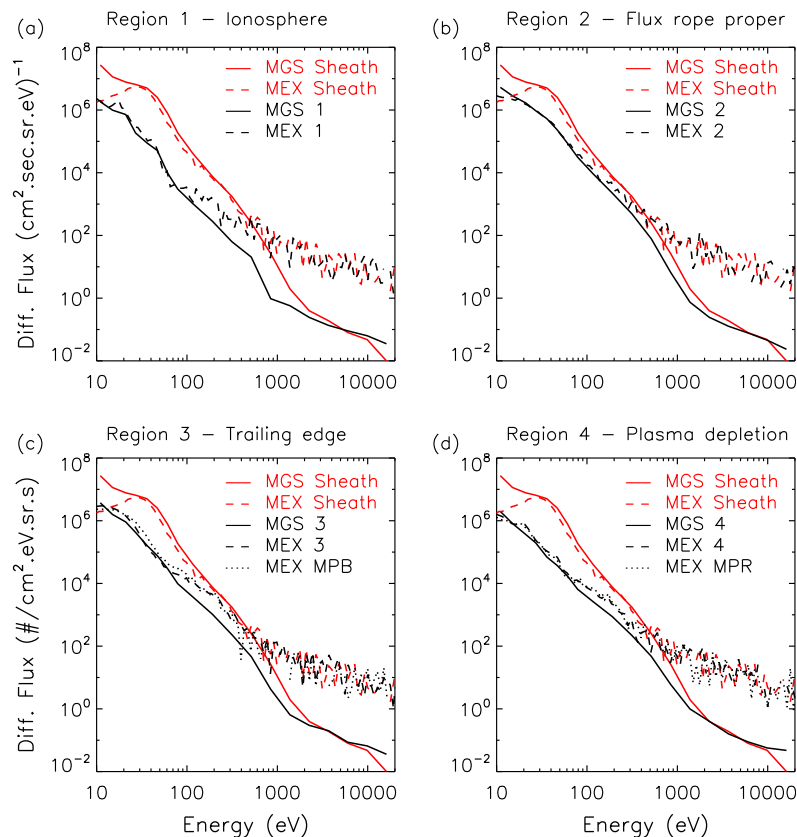


**Fig. 6.** (a–d) Comparison of electron energy spectra measured by ER (solid line) and ELS (dashed line) from regions 1 to 4 in Figs. 2d and 5b respectively, with energy spectra of magnetosheath electrons (red) for example ER data and ELS data from inbound data of Fig. 5a (at 23:20:00 UT and not shown). (c–d) Further comparisons to ELS data from the MPB and MPR (dotted line) also from the inbound data at earlier UT of Fig. 5a than shown at 23:31:00 UT and 23:32:00 UT respectively. (For interpretation of the references to colour in this figure legend, the reader is referred to the web version of this article.)

ELS have observed a spatial distortion of the plasma boundaries that has remained quasi-steady over the 7 min between the MGS and MEX pass. A re-entry into the magnetosheath would be the simplest explanation for observing magnetosheath-like electrons during the flux rope followed by an MPR-like depletion when exiting the flux rope.

If not the result of a re-entry into the magnetosheath proper, the depletion region in electron measurements found when exiting the large-scale flux rope on the dayside of Mars, may represent similar properties to the large-scale flux ropes observed at the terminator of Mars. Morgan et al. (2011) interpreted similar regions observed by MEX ELS surrounding a flux rope at the terminator of Mars, as resulting from the torsional structure of the magnetic field. The rotating magnetic field elongates the distribution of electrons from the ionosphere and is further reduced if the electron beam moves out of the instrument plane. It is possible this could be the case for the observations presented here since the MGS pitch angle data does become limited to a narrow range of pitch angles in the depletion region, indicating the magnetic field and any field aligned electrons move out of the ER instrument plane.

As MEX passes the flux rope location, ELS observed changes to the electron energy distribution function as shown in Fig. 5b. Here we have used a method from Soobiah et al. (2013) to construct the energy distribution function of electrons with respect to the angle from the Mars nadir. We present the ELS electron energy distribution function with respect to the Mars nadir as MEX is without a magnetometer instrument capable of making vector measurements of the magnetic field to calculate pitch angle distributions. In this case 0° represents electrons travelling towards Mars and 180° represents electrons travelling away from Mars. The resulting energy distribution is presented against time and has been separated into the same four energy bins used to present the MGS MAG/ER pitch angle data in Fig. 2e. Areas shaded by white diagonal lines indicate parts of the distribution function that have the spacecraft in the field of view and where we have interpolated the data.

Fig. 5b shows that the energy distribution of electrons from the ionosphere (23:40:24 UT–23:41:04 UT) and from the depletion region (23:41:04 UT–23:42:04 UT) are moving away from Mars since the normalised flux of electrons is found mainly around 180° from the Mars nadir. However, as MEX is without a magnetometer it is not possible to determine if the electrons are on open or closed field lines. As MEX moves through the trailing edge of the large-scale flux rope (region 3 between 23:42:04 UT and 23:43:45 UT), the part of the electron energy distribution between 10 eV and 50 eV is similar to the ionosphere and has an asymmetry of electrons moving away from Mars. Once MEX has reached the flux rope proper (region 2 between 23:43:45 UT and 23:46:20 UT) the normalised flux increases for angles closer to the Mars nadir and adjacent to angles looking over the spacecraft. As a result the uninterrupted field-of-view has not resolved the presence of a loss cone and the interpolation gives a more isotropic distribution over parts of the field-of-view looking over the spacecraft. The normalised flux close to 180° remains enhanced and by comparing to the pitch angle data from MGS in Fig. 2e, may correspond to a field aligned electron beam at low energies. ELS also observes a significant contribution to the energy distribution from electrons with energies between 50 eV and 100 eV, however seems to be in contrast to the electrons at lower energies. A missing component is present near 180° travelling away from Mars and an increased component of electrons near 90°. Note, both components are resolved by ELS sectors that do not have the spacecraft in the field of view. By comparing to the pitch angle data from MGS in Fig. 2e, the missing component of higher energy electrons measured by ELS around 180° away from Mars, would correspond with the loss cone, and the increased component near 90° would correspond to the trapped electrons measured by MAG/ER at this location. Therefore, the electron energy distributions generated by ELS supports MAG/ER observations for the simultaneous trapping of higher energy electrons and field aligned lower energy electrons at the location of the large-scale flux rope.

The electron energy distribution measured by ELS in the trailing edge of the large-scale flux rope (region 3) shows that between 10 eV and 50 eV, an enhanced flux of electrons is present near the perpendicular/horizontal to Mars. At the same time the electron flux between 50 eV and 100 eV, is contained in a narrow region of angles directed away from Mars and is observed alongside a depletion of flux directed at angles towards Mars. Note, these components are resolved by ELS sectors that do not have the spacecraft in the field of view. This indicates a reversal of the electron energy distribution measured near the centre of the large-scale flux rope (region 2). There is a suggestion of this in the MGS pitch angle data, as the enhanced field aligned electron flux between 10 eV and 50 eV can be observed to evolve towards more perpendicular/trapped pitch angles (after 23:39:02 UT in Fig. 2e). Whereas the electrons measured by ER at higher energies can be observed to change from a trapped pitch angle distribution to a more isotropic pitch angle distribution (after 23:39:25 UT in Fig. 2e).

Therefore, the dual spacecraft observations presented here by MGS MAG/ER and MEX ELS in the region of a large-scale flux rope on the dayside of Mars, shows that the dynamics of the plasma within the flux rope is highly localised changing spatially, yet is temporally stable over the duration of 7 min between each spacecraft pass.

By combining measurements from ER and ELS from the flux rope proper and trailing edge regions of the large-scale flux rope, we arrive at a rough estimate for the flux rope radius of 200 km. This estimate and the results of minimum variance analysis in Fig. 4 are used to provide a possible configuration of the large-scale flux rope as shown in Fig. 7. A radius of 200 km is similar to previous estimates obtained from force free models of large-scale flux ropes observed at the terminator of Mars (Brain et al., 2010; Beharrell and Wild, 2012). However, Fig. 7 shows a configuration for a large-scale flux rope not demonstrated by previous studies. Rather than having an axial direction tangential to the Mars horizontal, Fig. 7 shows the axial direction of the large-scale flux rope points towards Mars. Therefore, it might be possible for one end of the large-scale flux rope to interact with ionosphere/atmosphere at low altitudes.

### 3.3. Dayside current sheet region and plasma boundary on repeated MGS orbits

We have also conducted further analysis using MAG/ER observations of six consecutive MGS orbits (three before and three after) that repeated the same path taken by MGS through the location of the large-scale flux rope. Figs. 8 and 9 show the MAG/ER data of the consecutive passes that are separated by 88 orbits (~7 martian days) before and after the pass with the large-scale flux rope, which is presented on the fourth row of panels. It is evident that no other large amplitude enhancements of the magnetic field occur in the MAG data from the repeat passes before and after the event during this time frame. Therefore, the large-scale flux rope signature presented in this paper is a transient event and follows a similar result from Morgan et al. (2011). However, on each occasion there is a positive $B_y$ component in the draped magnetic field measured in the ionosphere at later UT (latitudes north of the strong crustal magnetic fields for the 7th, 14th and 21st July, 2006 and 5th and 13th August, 2006), there is a reversal in the magnetic field vectors ($B_x$ and $B_y$) closer to the region of crustal magnetic field, showing current sheet reversals similar to that
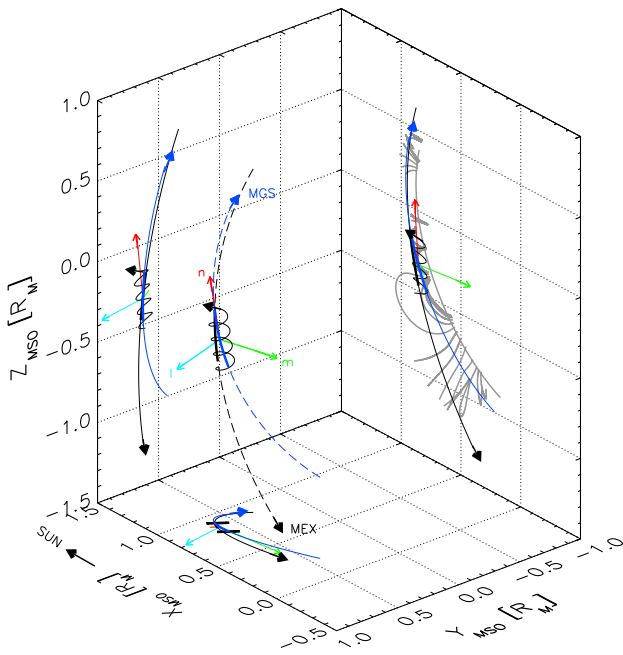
**Fig. 7.** Schematic of the large-scale flux rope signature measured by MGS MAG on 21st July, 2006, represented using MSO coordinates in a three-dimensional plot box. The estimated flux rope radius of ≈200 km is determined using the orbit path of MGS (solid blue line) and MEX (solid black line) through the regions of the flux rope proper and trailing edge (regions 2 and 3 in Figs. 2 and 5 respectively). Minimum variance analysis from Fig. 4 gives the flux rope orientation, where the axial direction of the flux rope is given by the minimum variance direction, $n$ (red arrow). Also shown is the maximum variance direction, $l$ (cyan arrow) and intermediate variance direction, $m$ (green arrow). Crustal magnetic fields obtained from the Cain model are traced along the orbit path of MGS (grey) and projected on to the $X_{MSO} - Z_{MSO}$ plane. (For interpretation of the references to colour in this figure legend, the reader is referred to the web version of this article.)

observed during the large-scale flux rope (identified by the dashed vertical lines in Figs. 8 and 9).

On all MGS orbits repeating the path taken through the location of the large-scale flux rope, ER observes a change in plasma by an increase in the differential flux of electrons above 100 eV (identified by the solid vertical lines in Figs. 8 and 9) as MGS moves from regions of ionosphere dominated by crustal magnetic fields to regions dominated by draped solar wind magnetic field. The location of this plasma boundary is also coincident with the measured magnetic field tending towards strengths almost twice that of the magnetic field obtained from the Cain model (presented by the right-hand vertical axis and dashed line of the left hand column of Fig. 8). The large-scale flux rope on the 21st July, 2006, represents the current sheet crossing that occurred closest to this boundary and also associated with the highest magnetic field strength measured in the ionosphere at later UT (latitudes north of the strong crustal magnetic fields).

As well as the magnetic field reversal in the $B_x$ and $B_y$ components, the current sheet crossings that occur on 5th and 12th August, 2006, have an additional enhancement in the $B_z$ component as shown in Fig. 8. The $B_z$ component and the magnetic field strength increases to a maximum as the $B_x$ and $B_y$ components reverse direction (09:03:34 UT on 5th August, 2006, and 13:44:58 UT on 12th August, 2006).

Fig. 10 plots the magnetic field measurements of the current sheet crossings (middle and right hand column of panels) that occurred on repeated MGS orbits after the large-scale flux rope (left hand column of panels) in minimum variance coordinates. Fig. 10 shows the large-scale flux rope and the current sheet crossings that occurred after the large-scale flux rope, share common features in the MVA coordinate frame: as the magnetic field along the

maximum variance direction reverses sign there is an increase in magnetic field along the intermediate variance direction until a peak is reached near the centre of the crossing, while the magnetic field along the minimum variance direction remains small and of the same sign. The hodograms of the middle and bottom row of Fig. 10 shows a rotation of magnetic field greater than >180° associated with the large-scale flux rope, whereas the current sheet crossings show a C-shape hodogram in the $l - m$ plane for a rotation of nearly ∼180°. The same properties of magnetic field in the minimum variance reference frame appear during tangential current sheet crossings that often occur at the Earth's magnetopause (Berchem and Russell, 1982). In a tangential current sheet, the magnetic field is everywhere parallel to the current sheet plane and is allowed to rotate tangentially within the current sheet plane rather than in the direction normal to that plane. This would be the case for the current sheet crossing that occurred after the large-scale flux rope and presented in Figs. 8 and 10, if the intermediate variance direction was along the current sheet plane. However, if comparing to the results of the large-scale flux rope, only magnetic field along the minimum variance direction does not change sign, indicating this as the direction of the flux rope axis and one of the MVA axes present in the current sheet plane. As the axis of the maximum variance represents the reversal of the magnetic field direction over the current sheet, it would suggest that in the case of the large-scale flux rope at least, the intermediate variance direction would be the MVA axis most likely normal to the current sheet plane.

The pitch angle data presented in Fig. 9 supports the current sheet crossings are of a similar structure to the large-scale flux rope signature on the 21st July, 2006. During the current sheet crossing between 09:01:10 UT and 09:04:20 UT on the 5th August, 2006, the electron differential flux is enhanced compared to the ionosphere and is similar to electrons measured during the large-scale flux rope signature, but at a slightly lower differential flux. Electrons measured during the current sheet crossings also have pitch angles like that observed during the large-scale flux rope. At lower energies electrons have a strong field aligned distribution and at higher energies electrons have a strong trapped pitch angle distribution. However, unlike the large-scale flux rope signature, a significant population of electrons at higher energies are more field aligned. Electrons are also observed at more intermediate pitch angles between perpendicular and field aligned, that is more conical. Hence, the current sheet crossing of 5th August, 2006, seems to show a different stage of the flux rope development. Furthermore, the energy spectra of electrons during the first part of the current sheet crossing remains ionospheric-like, whereas the remainder of the current sheet crossing shows enhanced differential flux as would indicate a magnetosheath-like population.

The current sheet crossing from 13:42:10 UT to 13:47:05 UT on the 12th August, 2006, seems to represent yet a further stage in the development of the flux rope. During this current sheet crossing, the energy spectrum of the electron differential flux is similar to the ionospheric plasma at later UT (at more northern latitudes). Although there are some fluctuations in the differential flux between 20 eV and 40 eV below and above the average. The pitch angles show the electrons primarily remain field aligned at both lower and higher energies. However, the field aligned electrons at lower energies are constrained to more narrow range of pitch angles and broadens out over a larger range in pitch angles as the energy increases. In addition, as the energy increases there is also the appearance of a lower flux of electrons at pitch angles just greater than perpendicular and loss of electrons at surrounding pitch angles.

### 3.3.1. Dayside trapping regions on open radial crustal magnetic field

The inbound sections (earlier UT) of Figs. 8 and 9 show regions dominated by a radial crustal magnetic field (Figs. 8a–d and g–j, 9a–d and g–j) also consist of electrons that are simultaneously field
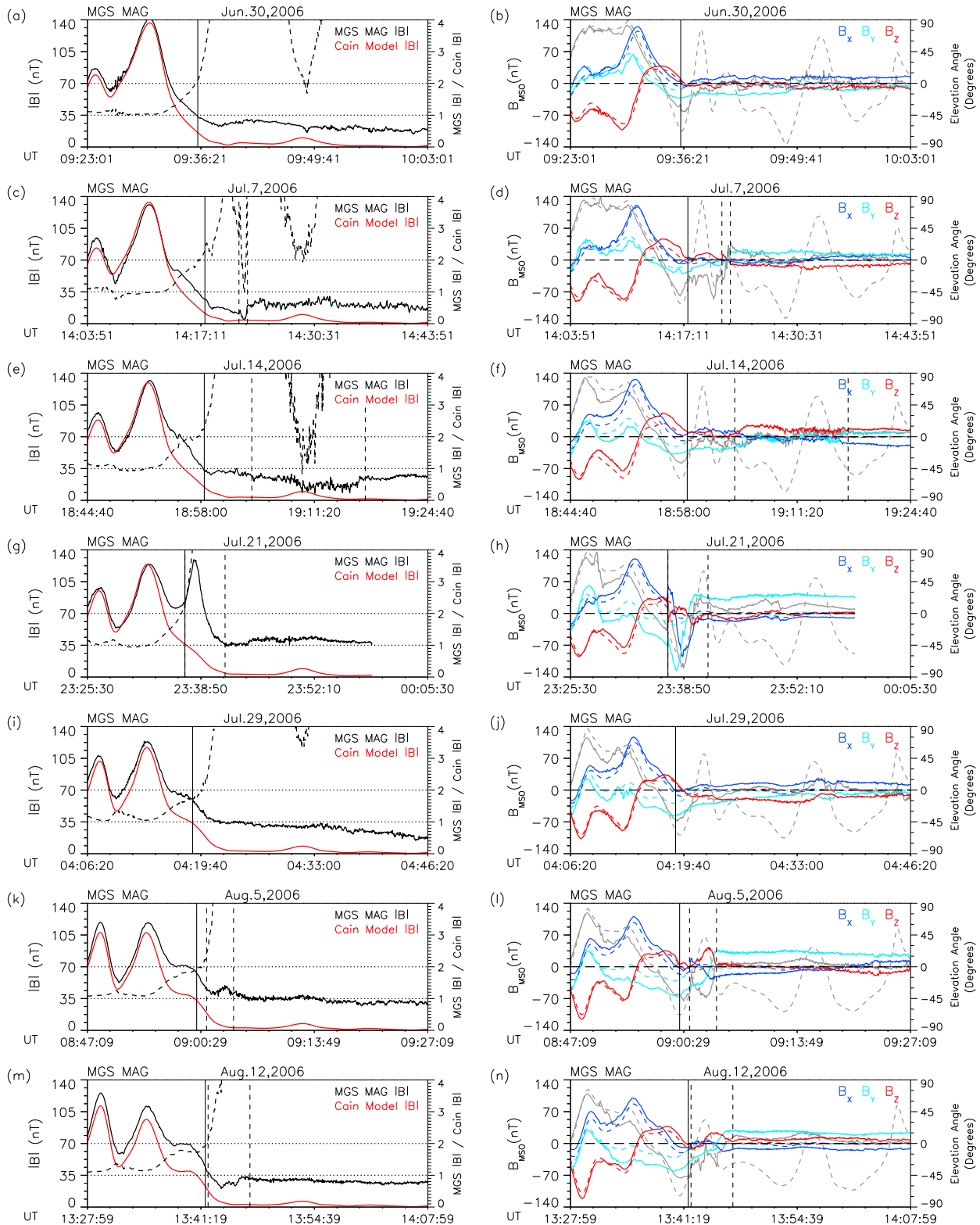
**Fig. 8.** Comparison of MAG data from consecutive MGS passes that repeat the same path over Mars taken by MGS on 21st July 2006 (shown by panels g and h) when MAG measured a large amplitude enhancement in magnetic field. Panels on the left hand column also display the ratio of the measured magnetic field strength by MAG to that obtained from the Cain model (dashed line and left hand axis) and dotted horizontal lines to highlight ratios between 1 and 2. Panels on the right hand column also display the magnetic field elevation angle (coloured using a grey scale and left hand axis), the angle between the magnetic field direction and the local zenith, −90° directed towards Mars, 0° directed along the Mars horizontal and 90° directed away from Mars. (For interpretation of the references to colour in this figure legend, the reader is referred to the web version of this article.)

aligned at lower energies and perpendicular/trapped at higher energies. Therefore, demonstrating the same behaviour recorded during the large-scale flux rope and those current sheet crossings that occurred after the large-scale flux rope.

Electrons displaying trapped pitch angle distributions at energies greater than 100 eV have been previously observed in regions dominated by a radial crustal magnetic field on the nightside of Mars (Lillis et al., 2011). However, on that occasion electrons showed
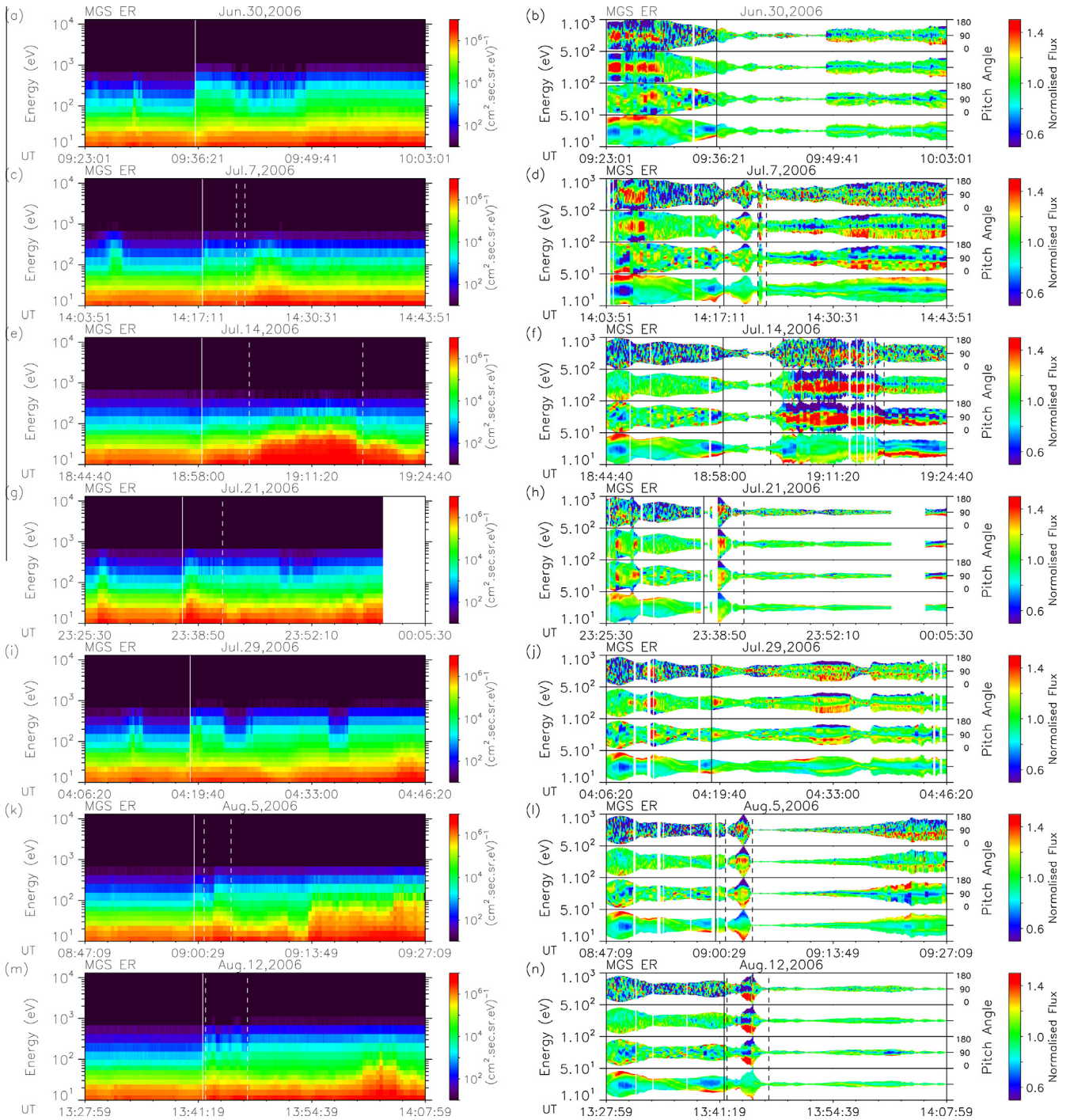
**Fig. 9.** Comparison of ER and pitch angle data from consecutive MGS passes that repeat the same path over Mars taken by MGS on 21st July 2006 (shown by panels g and h) when MAG measured a large amplitude enhancement in magnetic field.

trapped pitch angle distributions across both higher and lower energies, indicating the magnetic field was closed and not open.

### 3.3.2. Extended dayside current sheet crossing

The current sheet crossings recorded between 14:21:40 UT and 14:22:40 UT on the 7th July, 2006, and between 19:04:00 UT and 19:17:20 UT on the 14th July, 2006, (on the repeated MGS orbits prior to the large-scale flux rope), showed a depression in the magnetic field strength, until the magnetic field reached a minimum (14:22:19 UT and 19:09:58 UT respectively) and was close in strength to that of the crustal magnetic field obtained from the Cain model. Whereas, enhancements in magnetic field strength were measured during the large-scale flux rope and those current sheet crossings observed after large-scale flux rope. The reduction in the magnetic field strength measured during the current sheet crossings on repeated MGS orbits before the large-scale flux rope, is indicative MGS crossing close to the location of a neutral sheet.

The current sheet crossing on 14th July, 2006, displayed features not typical for a current sheet observed in the Martian ionosphere. On this occasion the magnetic field was observed to reverse direction over a 13 min period, during which strong fluctuations in the strength and direction of the magnetic field
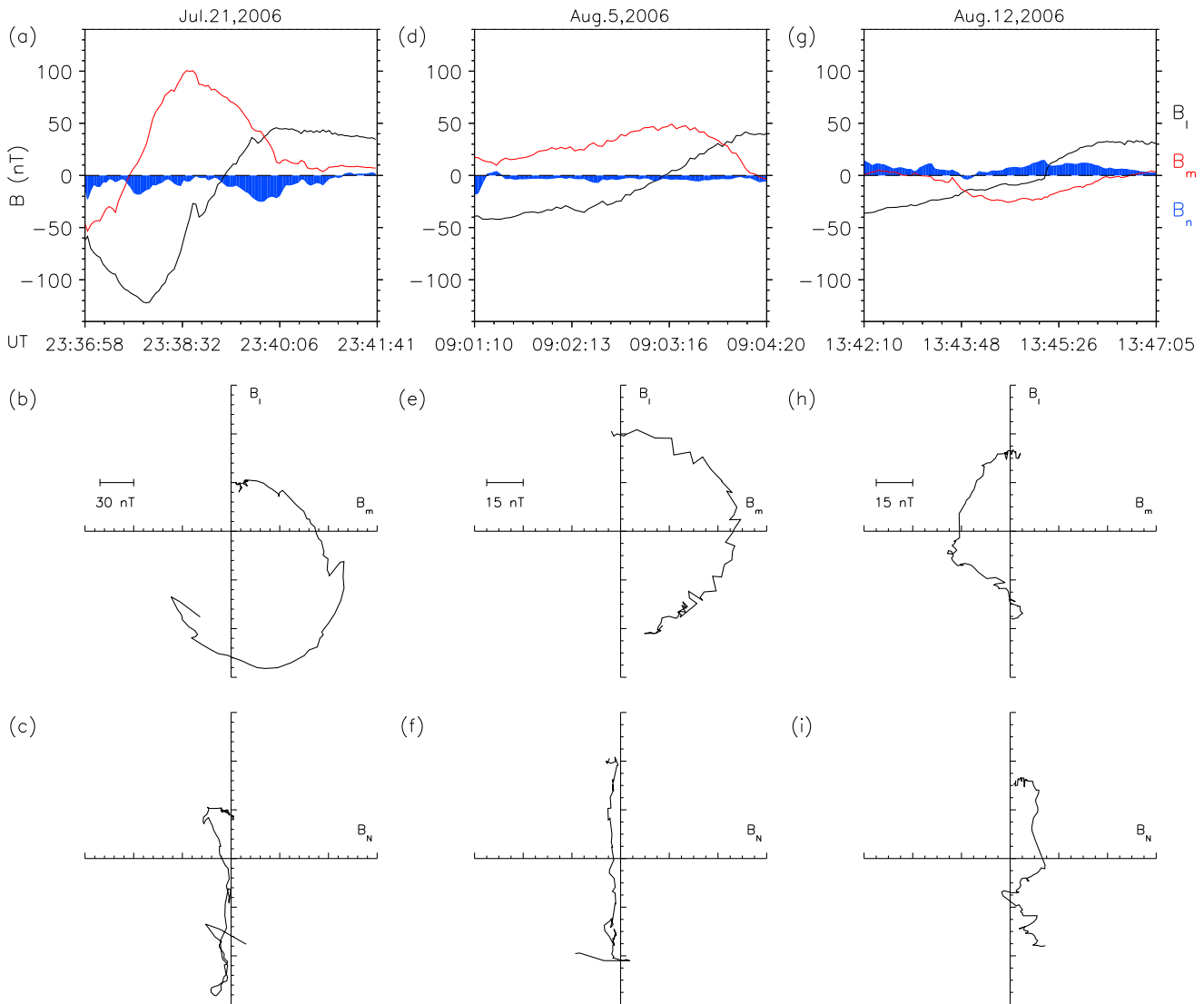
**Fig. 10.** MGS MAG data from the observation of the large-scale flux rope on the 21st July, 2006 and current sheet crossings on repeated MGS orbits on the 5th and 12th August, 2006, respectively, in MVA coordinate frame. Below, corresponding hodogram pairs in MVA coordinate frame are displayed: $B_l$, $B_m$ and $B_n$ corresponds to the magnetic field along the maximum, intermediate and minimum variance direction respectively.

were observed. A statistical study by Halekas and Brain (2010), of low altitude current sheets around Mars, found it takes <100 s to cross most current sheets and around 500 s (8 min 20 s) for the longest crossing. Therefore, in the case presented here MAG has observed a current sheet crossing that is exceptionally longer than has previously been reported for low altitudes at Mars. Given the MGS orbital velocity of 3.37 km/s and considering the current sheet as relatively stationary with respect to MGS, the current sheet presented here will have a thickness of approximately 2000 km (determined after taking into consideration the crossing angle of MGS with the current sheet). The thickness would only be smaller if the current sheet was moving in roughly the same direction as the spacecraft and at speeds equal to or less than the spacecraft. Such current sheet thickness is more characteristic of observations from Phobos 2 at higher altitude in the Mars induced magnetotail (Riedler et al., 1991; Yeroshenko et al., 1990). It is even more unusual for the dayside of Mars since the study by Halekas and Brain (2010) found that at low altitudes the average crossing time was slightly longer for night side current sheet crossings.

Fig. 9e shows that during the current sheet crossing (between 19:04:00 UT and 19:17:20 UT), ER measures electrons with an energy spectrum similar to that measured during the large-scale flux rope encounter; magnetosheath-like but with reduced differential flux. Fig. 9f shows that during the current sheet crossing (between 19:04:00 UT and 19:17:20 UT), electrons are simultaneously nearly field aligned at lower energies and trapped at higher energies, as was the case during the large-scale flux rope, current sheet crossings occurring after the large-scale flux rope and regions of radial crustal magnetic field.

Fig. 11 shows the MGS MAG/ER data of the extended current sheet crossing on 14th July, 2006 using an expanded horizontal axis. Fig. 11a and b shows that as well the standout ULF turbulence measured in the magnetic field of approximately 0.04 Hz (25 s), lower frequency fluctuations of approximately 0.003 Hz (330 s), are embedded in the $B_x$ and $B_y$ components. The lower frequency variation of the $B_x$ and $B_y$ components also shows the interesting property of being anti-correlated. Fig. 11c then shows that during the extended current sheet crossing, the largest increases in the integrated electron flux between energies of 30 eV–130 eV, and therefore plasma density and pressure, coincides with dips in the magnetic field strength. This indicates that possibly mirror mode waves are present in the plasma of the current sheet crossing.
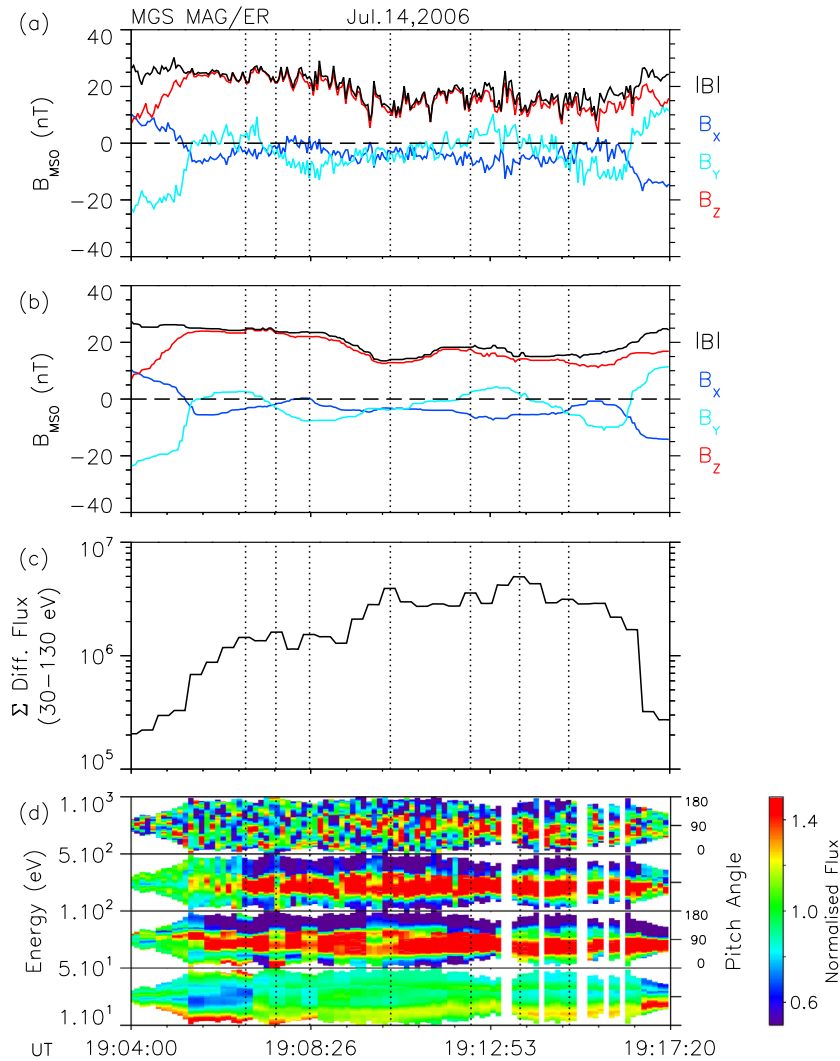
**Fig. 11.** MGS MAG/ER observations of an extended current sheet crossing on 14th July, 2006. (a) Magnetic field strength (black) and magnetic field vectors measured by MAG in MSO coordinates. (b) Smoothed magnetic field strength (black) and magnetic field vectors measured by MAG in MSO coordinates. (c) Integrated ER electron differential flux between 30 eV and 130 eV. (d) Electron pitch angle distribution separated into four energy bins. Dotted lines highlight times of maximums in the integrated differential flux of electrons.

## 4. Summary and discussion

We present dual spacecraft observations by MGS MAG/ER and MEX ASPERA-3 ELS of a large-scale magnetic flux rope on the dayside of Mars, which also occurs in close proximity to the crustal magnetic fields and a dayside current sheet region at Mars. The MGS MAG instrument observed a strong magnetic field enhancement of ~130 nT alongside a rotation and reversal of magnetic field vectors, indicating the presence of a large-scale flux rope within a current sheet crossing. The large-scale flux rope was also associated with an increase in the differential flux of electrons.

The MEX spacecraft passed the same region 7 min later, on an orbit path co-aligned with MGS, but moving southwards into the region of strong crustal magnetic fields. MEX ASPERA-3 ELS observed an almost identical energisation in electrons crossing the location of the large-scale magnetic flux rope and due to a higher-time resolution observed pulsations in the differential flux of electrons and the electron density, similar to the magnetosheath. Pitch angle distributions from MAG/ER near the centre of the large-scale flux rope showed the simultaneous presence of lower energy electrons aligned with the magnetic field and higher

energy electrons that were trapped. Corresponding features were also found in the electron energy distribution functions measured by ELS near closest approach to the flux rope location measured by MGS MAG.

The presence of trapped electrons observed during the large-scale flux rope on the dayside of Mars might suggest properties similar to the large-scale flux ropes studied at the terminator of Mars by Brain et al. (2010) and Morgan et al. (2011), where plasma inside the flux rope was isolated from surrounding ionosphere and contained on closed field lines. However, simultaneous observations of lower energy electrons that are field aligned within the large-scale flux rope, suggest that the field lines of the flux rope are open.

The progression from field aligned electrons at lower energies to trapped electrons at higher energies, is an indication of a pitch angle diffusion process taking place as MGS moves through the flux rope structure. Uluşen et al. (2011) reported a similar process taking place as MGS passed through boundary regions between open and closed crustal magnetic fields on the nightside of Mars. The authors suggested that electrons at lower energies could be accelerated by perpendicular or oblique heating, and as a result the electrons would reflect back at higher energies (see Uluşen et al.

(2011) and references therein). Perpendicular or oblique heating of electrons can result from the presence of upper hybrid waves that propagate nearly perpendicular to the background magnetic field (Wong et al., 1988). The upper hybrid waves can be excited by a population of warm electrons with a loss cone type distribution in a two-component (cold and warm) electron plasma (Wong et al., 1988).

The observation of field aligned electrons is also indicative of field aligned currents that could cause deflections in the magnetic field vectors, as was detected during the flux rope. The formation of a magnetic flux rope is often associated with the process of magnetic reconnection, which can generate field aligned currents (Saunders et al., 1984). Field aligned currents can also result in flux ropes since a flowing current will form a poloidal magnetic field analogous to that of a current-carrying wire, which will then encircle the original magnetic field creating a flux rope like signature. Furthermore, the minimum energy state of the helical magnetic field of a flux rope is represented by the "force-free" condition (Priest, 1990), which readily supports the existence of field aligned currents. This is because the magnetic force inside the flux rope, $J \times B$, equals zero when the current vector is everywhere parallel or anti-parallel to the magnetic field vector.

A force-free flux rope can remain stable in the MHD regime if pressure is conserved, as typically related to regions of low plasma beta, $\beta$, (ratio of thermal plasma pressure to magnetic pressure) (Burlaga, 1988). However, flux ropes can deviate from the force-free state in a continuum of forms (Elphic, 1980). As with large-scale flux ropes that occur at the terminator of Mars (Harnett, 2009; Brain et al., 2010), the large-scale flux rope observed here on the dayside of Mars is associated with an increase in electron differential flux and density near the flux rope axis. As a result, indicates a non-force-free flux rope that is not in equilibrium with the surrounding regions. We have been unable to confirm this by comparing to a best-fit force-free flux rope model, as it has not been possible to model the large-scale flux rope observed by MGS MAG on 21st July, 2006.

The observation of magnetosheath-like electrons alongside magnetosheath-like fluctuations in electron density during the large-scale flux rope, as well as electron energy spectra similar to the MPB and MPR when exiting the large-scale flux rope, suggested a re-entry into the magnetosheath due to a quasi-steady distortion of the plasma boundaries. However, it is not immediately apparent how some properties of the large-scale flux rope agree with this paradigm:

(1) The magnetic field from a large-scale flux rope is unlike magnetic field from the magnetosheath, which is usually associated with greater turbulence as shown by increased variability in the orientation and strength of the magnetic field (Bertucci et al., 2004). If considering the draped solar wind magnetic field on the dayside of Mars, the magnetic field is usually orientated close to the horizontal above Mars (Crider et al., 2004). Fig. 2c shows the magnetic field elevation angle during the crossing of the large-scale flux rope decreases steadily to become more radial. In this case, the variation of the magnetic field elevation angle is similar to that of the crustal magnetic field from the Cain model, suggesting a closer relationship to the crustal magnetic fields instead of magnetic field from the magnetosheath or draped solar wind.

(2) The peak in magnetic field strength of ∼130 nT during the large-scale flux rope is unlike that found in the magnetosheath, which is of the order of a few tens of nT. Also, the dayside compressed draped solar wind magnetic field can produce differences of 15–60 nT between measurements and a crustal magnetic field model (Cain et al., 2003).

(3) The depletion region in electron measurements found when exiting the large-scale flux rope, displays none of the enhanced magnetic field strength or change in orientation expected of a pile-up region (Bertucci et al., 2004).

(4) The trapped pitch angle distribution of electrons >100 eV observed during the large-scale flux rope is unlike the isotropic pitch angle distribution typical of magnetosheath electrons.

Given the conflict in evidence that a re-entry into the magnetosheath is responsible for the properties observed during the large-scale flux rope, the remainder of the discussion will consider other possibilities that can better explain for the properties of the magnetic field and electron measurements during the large-scale flux rope.

Repeated orbits of the MGS spacecraft revealed the large-scale flux rope signature was observed in the vicinity of a dayside current sheet associated with similar rotations in MSO coordinates to that of the large-scale flux rope signature, as well as a $+B_y$ component in the draped solar wind magnetic field present in the ionosphere at later UT (latitudes north of the strong crustal magnetic fields). Also, all MGS orbits repeating the path taken through the location of the large-scale flux rope, show evidence of a plasma boundary by the decrease in electron differential flux above 100 eV when moving into regions dominated by the crustal magnetic field. The magnetic field strength measured by MAG at this boundary is found to be almost twice that of the magnetic field obtained from the Cain model. The contribution to magnetic field measured on the dayside of Mars from external sources will depend on factors that vary in time when responding to the changing conditions present in the ionosphere. Therefore, it is unlikely magnetic fields from external sources can repeat so precisely to match the crustal magnetic field at the plasma boundary for the seven consecutive repeated orbits, while the draped solar wind magnetic field measured in the ionosphere shows different magnetic field strengths and orientation. Instead, these observations seem to suggest properties expected of a magnetopause that forms to separate two regions of distinct plasma and frozen-in magnetic field, where the boundary surface represents the balance of pressure between the two regions.

At Mars the plasma boundary would represent a type of "mini-magnetopause", separating regions of the crustal magnetic field from regions dominated by the draped solar wind magnetic field that has advected into the ionosphere. Here the balance of pressure will involve a combination of dynamic plasma pressure, thermal plasma pressure and the magnetic field pressure in both regions. As in the case of magnetospheres like the Earth, we seem to observe a similar pressure balance surface since the measured magnetic field reaches strengths equal to almost double the undisturbed crustal magnetic field found at the location of the plasma boundary. This could be explained if due to the combination of the magnetic field from the mini-magnetopause current sheet and the background field either side of the mini-magnetopause.

Unlike the Earth, the gyroradius of the solar wind ions and the planetary ions from the martian ionosphere is on the same scale or larger than that of the crustal magnetic field structures and therefore would not satisfy the conditions for ideal MHD, required for the formation of a magnetopause. However, non-ideal MHD simulations by Harnett and Winglee (2003) demonstrates that a magnetopause-like structure may form in place of an MPB, when the solar wind interacts with strong crustal magnetic fields from the southern hemisphere of Mars. Unfortunately, the study did not include results at lower altitudes between regions of ionosphere dominated by magnetic field from the crust and regions dominated by the draped solar wind magnetic field that has advected into the ionosphere. Hence, further efforts are required

to develop both non-ideal MHD models (Harnett and Winglee, 2003) and ideal MHD models (Ma et al., 2002) of the solar wind interaction with the crustal magnetic fields of Mars, to establish a theoretical basis for the formation of a plasma boundary between regions of ionosphere dominated by magnetic field from the crust and regions dominated by the draped solar wind magnetic field that has advected into the ionosphere.

For examples where the draped solar wind magnetic field in the ionosphere is of a different orientation to the plasma boundary, observations show the presence of a current sheet changes the direction of the draped solar wind magnetic field to one similar to the plasma boundary. However, in all cases apart from the large-scale flux rope, the current sheet is not coincident with the plasma boundary and is instead located at some distance away. It is uncertain why this should be the case, as in the example of the Earth's magnetopause, there is only the current sheet located at the pressure balance boundary, where both solar wind and magnetospheric magnetic fields are reversed. On the occasion of the large-scale flux rope, the start of current sheet was coincident with the plasma boundary. In this example, the magnetic field strength and therefore pressure of the draped magnetic fields in the ionosphere was greater compared to observations of current sheets not coincident with the plasma boundary.

Obvious comparisons can be drawn for large-scale flux ropes that occur at a suspected mini-magnetopause type boundary on the dayside of Mars, with flux transfer events (FTE's) that occur on the dayside of the Earth's magnetopause. However, some differences apply since our observations at Mars are between a mini-magnetopause type boundary and the draped solar wind magnetic field in the ionosphere. Flux transfer events at the Earth occur between the magnetopause and the draped solar wind magnetic field in the magnetosheath. It is not known if the large-scale flux rope observed on the dayside of Mars is the result of intermittent reconnection at a martian mini-magnetopause or if other flux ropes would show a bi-polar signature along the boundary normal, as is the case for FTE's at the Earth's magnetopause (Russell and Elphic, 1978). Also, further investigation is required to determine the outcome of introducing newly open magnetic field flux on the dayside of Mars, for example, if, when and how the additional open magnetic field reconnects back to form closed magnetic field.

The magnetic field and electron pitch angle distributions measured during the current sheet crossings that occurred after the large-scale flux rope demonstrated similar magnetic field topology as the large-scale flux rope. The current sheet reversals also included an additional $+B_z$ enhancement similar to that measured during the large-scale flux rope. When represented in the MVA coordinates, the increase in magnetic field along the $B_z$ axis in MSO corresponded to an increase in the magnetic field along the intermediate variance direction. The intermediate magnetic field reaches a peak near the centre of the current sheet crossing, while the magnetic field along the minimum variance direction remains small and of the same sign. If in the current sheet plane, the magnetic field along the intermediate variance direction would represent a tangential rotation of magnetic field from a tangential current sheet. The l-m hodograms of the current sheet also reproduced the characteristic C-shape rotation of nearly ~180° observed during tangential current sheets at the Earth's magnetopause (Berchem and Russell, 1982). However, this disagrees with the minimum variance analysis of the large-scale flux rope, which identified the minimum variance direction as the most likely direction of the flux rope axis. Therefore, if the maximum and minimum variance directions represent the two MVA axes of the current sheet plane, would indicate the intermediate variance direction is most likely normal to the current sheet plane of the large-scale flux rope.

In Fig. 7 showing the configuration of the large scale flux rope, the current sheet plane is close to the YZ plane in MSO and at an angle to the Mars horizontal, whereas the normal direction points along the $-X$ direction in MSO and towards Mars. The MVA analysis of the current sheets that occurred after the large-scale flux rope provided direction eigenvectors for the maximum variance of $l = -0.46,\ 0.86,\ 0.21)$ and $(-0.33,\ 0.91,\ 0.23)$ (mostly along $+Y$ in MSO), the intermediate variance of $m = (-0.31,\ -0.38,\ 0.87)$ and $(-0.25,\ 0.15,\ -0.96)$ (mostly along $+/-Z$ in MSO) and the minimum variance of $n = (0.83,\ 0.33,\ 0.44)$ and $(-0.91,\ -0.37,\ 0.18)$ (mostly along $+/-X$ in MSO). This shows a comparable orientation to the large-scale flux rope, where the current sheet plane, the intermediate (normal) and minimum variance direction have rotated around the maximum variance direction which remains mostly fixed along $+Y$ in MSO. This suggests that the peak magnetic field in the intermediate direction is along the current sheet normal rather than being tangential. Further information is required to determine the formation of the current sheet plane with respect to Mars and a possible mini-magnetopause type boundary at the crustal magnetic field more accurately. In the case of the Earth magnetopause it is possible to determine which MVA direction is most likely to be normal to the magnetopause current sheet, as the corresponding axis would be the nearest to line from the Earth to the satellite (pointing away from or towards the Earth).

If not from a tangential rotation of the current sheet magnetic field, we must consider other possible contributions that could produce a peak in magnetic field along the intermediate direction. First, we consider the possible contribution from the crustal magnetic fields.

As well as being observed during the large-scale flux rope and the current sheet crossings that occurred after the large-scale flux rope, pitch angle distributions of simultaneous field aligned low energy electrons and trapped higher energy electrons were also common to regions of strong crustal magnetic fields that were mostly radial. This suggests the large-scale flux rope and the current sheet crossings share a common magnetic field topology to the radial magnetic field cusps from regions of strong crustal magnetic field. Indeed, the variation measured in the magnetic field vectors and magnetic field elevation angle during the large-scale flux rope (shown in Figs. 2b and 2c respectively), closely follows that from the Cain model of the crustal magnetic field. The magnetic field elevation angle during the large-scale flux rope becomes increasingly radial as the peak in the $B_z$ field component is reached. This suggests that part of the large-scale flux rope presented here on the dayside of Mars, involves radial crustal magnetic field lines from the edge of the strong crustal magnetic field region.

Similarly, the magnetic field measured during the two current sheet crossings that occurred after the large-scale flux rope showed elevation angles that become increasingly negative and less horizontal (more radial) as the peak in magnetic field along the $B_z$ direction is reached. As demonstrated by the pitch angle data, this suggest a similar configuration of magnetic field found during the large-scale flux rope is involved during the current sheet crossings. However, it is not immediately apparent why this should be the case, as the crustal magnetic fields from the Cain model nearest the centre of the two current sheet crossings have positive elevation angles compared to the measured negative elevation angle. Perhaps open crustal magnetic fields from stronger regions further south have stretched to more northern latitudes. However, if involving crustal magnetic fields from regions of negative radial field near 0° latitude, would result in a $-B_z$ magnetic field compared to the $+B_z$ field observed during the current sheet crossings that occurred after the large-scale flux rope. Crustal magnetic fields from more southern regions of positive radial field

(between latitudes of −6° and −37°) would result in a +$B_z$ when stretched to more northern latitudes. However, between 23:26: 30 UT and 23:29:25 UT in Fig. 9h, electrons from the southern region of positive radial crustal magnetic field are observed moving in the opposite direction along the magnetic field compared to electrons measured during the large-scale flux rope between 23:36:58 UT and 23:37:43 UT. Therefore, it does not seem likely open crustal magnetic field from more southern regions (positive or negative radial magnetic field) would account for the +$B_z$ enhancement and magnetic field peak along the intermediate variance direction during the current sheet crossings.

We now consider what possible contribution magnetic reconnection would make to the observation of the peak in magnetic field along the intermediate direction during the current sheet crossings.

Eastwood et al. (2008) and Halekas et al. (2009) identified from magnetic field observations at Mars, the signatures of the Hall magnetic field from the diffusion region of magnetic reconnection. This usually occurs as a bi-polar variation in magnetic field along the current sheet plane and perpendicular to the maximum variance direction, which has not been observed here. It is possible the presence of a guide field during magnetic reconnection could distort the Hall magnetic field to become less bi-polar (Huang et al., 2014) and form a peak in magnetic field similar to that observed during the current sheet crossings that occurred after the large-scale flux rope. Also, the disruption of the neutral sheet by magnetic reconnection can lead to the presence of axial magnetic fields (Altyntsev et al., 1977) and helical magnetic field structures within a current sheet (Gekelman et al., 1987). However, these magnetic fields signatures would typically be observed along the current sheet plane and apply to the minimum variance direction of the current sheet crossings.

It is possible for magnetic fields to occur in the direction normal to the current sheet plane, through the highly kinked magnetic fields present in the geometry of a reconnecting current sheet. Also, a normal component of magnetic field is also associated with magnetic reconnection under the presence of a guide field during a non-symmetric inflow (Eastwood et al., 2013). Therefore, the observation of a normal component of magnetic field during the current sheet crossings, as well as the large-scale flux rope, forms evidence of magnetic reconnection between crustal magnetic field and draped solar wind magnetic fields on the dayside at Mars. This is supported by large shear in magnetic field between the crustal magnetic field and the draped solar wind magnetic field, being more widespread when the draped magnetic field has a +$B_y$ component (not shown here). As the MGS orbits repeating the path taken through the location of the large-scale flux rope show an additional −$B_y$ magnetic field within the crustal magnetic field regions, the shear in magnetic field would be enhanced further. However, as neither the Hall magnetic field signature nor a null point in magnetic field are observed on any of the MGS orbits repeating the path taken through the location of the large-scale flux rope, indicates the location where magnetic reconnection takes place is away from the MGS orbit paths and most likely from adjacent regions of crustal magnetic field. By observing current sheets with a normal component of magnetic field on a number of orbits that repeat the same path indicates that magnetic reconnection in nearby regions occurs readily when the draped solar wind magnetic field has a +$B_y$ component and is also possibly quasi-steady/continuous. Or this could indicate the normal component of magnetic field introduced by reconnection into the current sheet is quasi-steady over long periods.

Magnetic reconnection could also be implicated in the observations of trapped magnetosheath-like electrons during the large-scale flux rope and the current sheet crossings that occurred after the large-scale flux rope. This is because the quadrupole arrangement of magnetic fields that make up the reconnection X-line region consists of a magnetic minimum that would allow the trapping of electrons (Egedal et al., 2008). However, a common-ality of electron pitch angle distributions measured during the large-scale flux rope, current sheet crossings and regions of radial crustal magnetic field, indicated a common magnetic field topology of open magnetic field from the crust. It is possible a quadrupole magnetic field arrangement may also form when the cusps of the crustal magnetic fields meet opposing magnetic field from the solar wind. Similar conditions are known to exist at the cusps of the Earth's polar magnetic field, where the minimum of the quad-rupolar magnetic field results in the trapping of energetic particles with near 90° pitch angles (Sheldon et al., 1998).

The current sheet reversal observed on the repeated MGS orbit prior to the large-scale flux rope, occurred over a 13 min period or thickness of approximately 2000 km if stationary. This extended current sheet crossing is exceptionally longer than has previously been reported for low altitudes at Mars. The current sheet crossing was observed with a depression in the magnetic field strength, until the magnetic field reached a minimum (close in strength to that of the crustal magnetic field obtained from the Cain model). At same time a large increase in the differential flux of electrons is observed. Therefore, the extended current sheet crossing contains plasma of higher density and temperature compared to the local ionosphere, while the magnetic field strength is gradually decreasing. This indicates that the region within the current sheet crossing experiences an increase in the local plasma pressure, whilst simultaneously experiencing decreasing pressure from the magnetic field. If the plasma pressure dominates over the magnetic field pressure, the region will become diamagnetic and a "bubble" in the magnetic field will begin to form and continue to expand until it is constrained by compressed and/or strained magnetic field lines.

Indeed, the turbulence of the magnetic field strength and orientation during the extended current sheet crossing is a feature shared with MAG observations of hot diamagnetic cavities upstream of the martian bow shock (Øieroset et al., 2001). These events at Mars are believed to result from the interaction of solar wind discontinuities with the bow shock and as such analogous to hot flow anomalies at Earth (Øieroset et al., 2001). However, we do not suggest this is the case here since the MAG observation presented in Fig. 8e and f is within the martian ionosphere, whereas hot flow anomalies are associated with the complex dynamics that arise in the foreshock region in front of the bow shock. Also, the extended current sheet crossing only involves a depression in magnetic field strength during the interval of turbulent field and is not flanked by large magnetic field enhancements observed at times of associated hot flow anomalies events at Mars (Øieroset et al., 2001). As such, our observation demonstrates properties of another form of current sheet referred to as a magnetic hole or magnetic bubble and would be the first time such a structure has been found in the ionosphere of Mars. Such structures have been identified in the solar wind (Turner et al., 1977; Fitzenreiter and Burlaga, 1978; Stevens and Kasper, 2007; Zhang et al., 2008a,b; Amariutei et al., 2011), in the Earth's magnetosheath (Kaufmann et al., 1970; Tsurutani et al., 1982; Hubert et al., 1989; Fazakerley and Southwood, 1994; Schwartz et al., 1996; Lucek et al., 1999) in the magnetosheath of Jupiter (Tsurutani et al., 1993; Balogh et al., 1992; Erdős and Balogh, 1996) in cometary plasma (Russell et al., 1987) and at the borders of the heliosphere (Tsurutani et al., 1992).

Magnetic holes are also known for being mirror mode structures. There is evidence this is also the case for the extended current sheet crossing observed prior to the large-scale flux rope. The highly anisotropic pitch angle distribution of the trapped electrons measured during the extended current sheet, is indicative of similar anisotropies in the plasma temperature of $T_\perp > T_\parallel$. If coinciding

with increased plasma density and therefore higher plasma beta, $\beta$, it may be possible for the plasma to satisfy the mirror mode instability and therefore support mirror mode waves. This is supported by the observation for the largest increases in the integrated differential flux of electrons between 30 eV and 130 eV, and therefore plasma density and pressure, coinciding with dips in the magnetic field strength as would occur in the presence of mirror mode waves. As the mirror mode instability is a collective mode that transfers magnetic energy to thermal energy perpendicular to the field, it could be an important factor for both the trapping of higher energy magnetosheath particles and the pitch angle diffusion of lower energy electrons in the region of the extended current sheet. It might be possible that similar conditions exist during the large-scale flux ropes and the current sheet crossings that occurred after the large-scale flux rope. However, the identification of mirror mode instability is far from confirmed as this would require more complete plasma measurements, such as moments of density and temperature from both electrons and ions. If this is found to be the case, the mirror mode waves present during the extended current sheet may set off compressions of the magnetic field that could evolve into sawtooth structures previously observed at Mars (Halekas et al., 2011).

Similar structures of depressed magnetic field are also observed in the high-altitude cusps regions of the Earth, as associated with the observations of cusp energetic particles (Chen and Fritz, 1998) and ULF wave activity (Nykyri et al., 2011). Therefore, if involving open crustal magnetic field, the observation of an extended current sheet and hot diamagnetic region at Mars could represent an analogy to the cusp diamagnetic cavities of the Earth. Recent developments by Nykyri et al. (2012), have demonstrated how high-energy particles in cusp diamagnetic cavities of the Earth may be created locally as a result of magnetic reconnection and perpendicular heating alone, rather than the trapping of magnetosheath particles. There is reason to believe properties found during the current sheet crossings that occurred on repeated MGS orbits after the large-scale flux rope and the extended current sheet crossing that occurred before, provide support of a similar process on the dayside of Mars.

In the example of the first current sheet crossing that occurred after the large-scale flux rope, similar pitch angle distributions were measured throughout the current sheet crossing despite a change in the electron energy spectrum, from electrons that were initially ionospheric-like, to more magnetosheath-like electrons measured in the later part of the current sheet. In the example of the extended current sheet crossing, Fig. 9f shows electrons with perpendicular pitch angles (between 50 eV and 500 eV) persist just after the extended current sheet crossing (between 19:17:20 UT and 19:21:16 UT) and evolve towards more field aligned directions with increasing UT. Also during this period, the differential flux of electrons is in-between differential fluxes measured during the extended current sheet crossing and the ionosphere (between 18:59:00 UT and 19:17:20 UT). This is unlike the typical energy spectra of the dayside magnetosheath, which would involve a greater differential flux of electrons than measured during the extended current sheet. Instead, the energy spectrum during this time is closer to that of the ionosphere, suggesting an energisation/heating of the local electron population. Note, the magnetic field measurements at this time only showed properties of a current sheet crossing of draped solar wind magnetic field and showed no indication of passing through the MPB or MPR region that would result from a re-entry into the magnetosheath. Therefore, this supports results from Nykyri et al. (2012), where common pitch angle distributions connect the perpendicular hot component within the diamagnetic cavity to regions of the surrounding ionosphere.

In the case of the extended current sheet crossing, ULF fluctuations observed in the magnetic field may act as a source of energy to accelerate electrons. Lower frequency fluctuations of approximately 0.003 Hz (330 s) were found embedded within the magnetic field vectors showing the current sheet rotation ($B_x$ and $B_y$ component), indicating either temporal changes from the movement of the current sheet position over the spacecraft, or spatial changes as the spacecraft crossed different sides of the current sheet. Nykyri et al. (2011) proposed that a similar property observed in diamagnetic cavities at the cusp regions of the Earth's magnetosphere as responsible for accelerating particles.

The simultaneous measurement of lower energy field aligned electrons and higher energy trapped electrons in the regions of the large-scale flux rope, current sheet crossings, radial crustal magnetic field and also the extended current sheet, show pitch angle diffusion or perpendicular heating as a route to accelerate electrons locally and reflect back into more perpendicular pitch angles at higher energies. Previous studies have demonstrated that perpendicular heating is an important aspect of particle dynamics of the crustal magnetic field cusps (Nielsen et al., 2007; Zou et al., 2010; Uluşen et al., 2011) and auroral regions at Mars (Lundin et al., 2006a,b; Dubinin et al., 2009), and may be the combination of heating from impacting precipitating electrons/solar wind particles, wave–particle interactions and magnetic mirroring effects. The evidence presented in this paper adds further support to wave–particle interactions as an important feature of open crustal magnetic fields on the dayside of Mars.

However, without the monitoring of upstream conditions and a larger number of simultaneous multi-point observations in regions above and adjacent to the dayside current sheets and large-scale flux rope, it is uncertain how much of a contribution local heating/acceleration processes would make to the observations of energetic electrons within these structures. Therefore, we must consider that the observations of magnetosheath-like electrons of reduced differential flux in regions of the large-scale flux rope, dayside current sheets and also radial crustal magnetic fields, are the result of some connection to the magnetosheath. Most likely due to magnetic reconnection between crustal magnetic fields and draped solar wind magnetic field, either in the ionosphere or magnetosheath.

## 5. Conclusions

We conclude observations by MGS MAG/ER and MEX ASPERA-3 ELS of a large-scale flux rope during a reversal of magnetic field vectors, that occurred in close proximity to MGS MAG/ER observations of a dayside current sheet region and plasma boundary, occurring on repeated MGS orbits, represents evidence of magnetic reconnection at a mini-magnetopause type boundary at Mars. Reconnection takes place between crustal magnetic fields and draped solar wind magnetic field either in the ionosphere or magnetosheath. The mini-magnetopause type boundary is required to separate regions of ionosphere dominated by crustal magnetic field from ionosphere dominated by the draped solar wind magnetic field. Our observations indicate the effects of magnetic reconnection at the mini-magnetopause type boundary or a quadrupole magnetic field trap around open crustal magnetic fields drives large scale dynamics in the martian ionosphere. Similar processes at other planets are usually associated in regions beyond the ionosphere between the shocked solar wind and the planet's magnetosphere. Our observations show the association of different plasma wave processes with the current sheets and large-scale flux rope that occurred at the perimeter of the dayside crustal magnetic field. As a result, could be an important factor to consider in the evolution of the martian atmosphere and provides exciting new areas for study in future MAVEN and MEX investigations at Mars.

## Acknowledgments

## References

Acuña, M.H. et al., 1999. Global distribution of crustal magnetization discovered by the Mars Global Surveyor MAG/ER experiment. Science 284, 790–793.

Altyntsev, A.T., Krasov, V.I., Tomozov, V.M., 1977. Magnetic energy dissipation in neutral current sheets. Sol. Phys. 55, 69–81.

Amariutei, O.A., Walker, S.N., Zhang, T.L., 2011. Occurrence rate of magnetic holes between 0.72 and 1 AU: Comparative study of Cluster and VEX data. Ann. Geophys. 29, 717–722.

Balogh, A. et al., 1992. Magnetic field observations during the Ulysses flyby of Jupiter. Science 257, 1515–1518. http://dx.doi.org/10.1126/science.257.5076.1515.

Barabash, S., et al., 2004. ASPERA-3: analyser of space plasmas and energetic ions for Mars Express. In: Wilson, A., Chicarro, A. (Eds.), Mars Express: The Scientific Payload, European Space Agency Special Report SP-1240, European Space Agency Research and Scientific Support, European Space Research and Technology Centre, Noordwijk, The Netherlands, pp. 121–139.

Beharrell, M.J., Wild, J.A., 2012. Stationary flux ropes at the southern terminator of Mars. J. Geophys. Res. 117, A12212. http://dx.doi.org/10.1029/2012JA017738.

Berchem, J., Russell, C.T., 1982. Magnetic field rotation through the magnetopause: ISEE 1 and 2 observations. J. Geophys. Res. 87, 8139–8148.

Bertucci, C. et al., 2004. MGS MAG/ER observations at the magnetic pileup boundary of Mars: Draping enhancement and low frequency waves. Adv. Space Res. 33, 1938–1944.

Brain, D.A. et al., 2006a. On the origin of aurorae at Mars. Geophys. Res. Lett. 33, L01201. http://dx.doi.org/10.1029/2005GL024782.

Brain, D.A., 2006b. Mars Global Surveyor measurements of the martian solar wind interaction. Space Sci. Rev. 126, 77–112.

Brain, D.A., Luhmann, J., Halekas, J., Frahm, R., Winningham, D., Barabash, S., 2006c. Simultaneous Mars Express/MGS observations of plasma near Mars. 2006 AGU Fall Meeting Abstracts. A8.

Brain, D.A., Lillis, R.J., Mitchell, D.L., Halekas, J.S., Lin, R.P., 2007. Electron pitch angle distributions as indicators of magnetic field topology near Mars. J. Geophys. Res. 112, A09201.

Brain, D.A. et al., 2010. Episodic detachment of martian crustal magnetic fields leading to bulk atmospheric plasma escape. Geophys. Res. Lett. 37, 14108.

Briggs, J.A., Brain, D.A., Cartwright, M.L., Eastwood, J.P., Halekas, J.S., 2011. A statistical study of flux ropes in the martian magnetosphere. Planet Space Sci. 59, 1498–1505.

Burlaga, L.F., 1988. Magnetic clouds and force-free fields with constant alpha. J. Geophys. Res. 93, 7217–7224.

Cain, J.C., Ferguson, B.B., Mozzoni, D., 2003. An $n = 90$ internal potential function of the martian crustal magnetic field. J. Geophys. Res. 108, 5008.

Chen, J.S., Fritz, T.A., 1998. Correlation of cusp MeV helium with turbulent ULF power spectra and its implications. Geophys. Res. Lett. 25, 4113–4116.

Crider, D.H. et al., 2004. Mars Global Surveyor observations of solar wind magnetic field draping around Mars. Space Sci. Rev. 111, 203–221.

Dubinin, E. et al., 2009. Long-lived auroral structures and atmospheric losses through auroral flux tubes on Mars. Geophys. Res. Lett. 36, 8108.

Eastwood, J.P. et al., 2008. Geophys. Res. Lett. 35, 2106.

Eastwood, J.P., Videira, J.J.H., Brain, D.A., Halekas, J.S., 2012. A chain of magnetic flux ropes in the magnetotail of Mars. Geophys. Res. Lett. 39, L03104. http://dx.doi.org/10.1029/2011GL050444.

Eastwood, J.P. et al., 2013. Influence of asymmetries and guide fields on the magnetic reconnection diffusion region in collisionless space plasmas. Plasma Phys. Control. Fusion 55, 124001–124006. http://dx.doi.org/10.1088/0741-3335/55/12/124001.

Egedal, J. et al., 2008. Evidence and theory for trapped electrons in guide field magnetotail reconnection. J. Geophys. Res. 113, 12207.

Elphic, R.C., 1980. Observations of the dayside ionopause and ionosphere of Venus. J. Geophys. Res. 85, 7679–7696. http://dx.doi.org/10.1029/1980JA085iA13p0767.

Elphic, R.C., Russell, C.T., 1983. Global characteristics of magnetic flux ropes in the Venus ionosphere. J. Geophys. Res. 88 (A4), 2993–3003.

Erdős, G., Balogh, A., 1996. Statistical properties of mirror mode structures observed by Ulysses in the magnetosheath of Jupiter. J. Geophys. Res. 101, 1–12.

Espley, J.R., Cloutier, P.A., Brain, D.A., Crider, D.H., Acuña, M.H., 2004. Observations of low-frequency magnetic oscillations in the Martian magnetosheath,

magnetic pileup region, and tail. J. Geophys. Res. 109, A07213. http://dx.doi.org/10.1029/2003JA010193.

Espley, J.R., Cloutier, P.A., Crider, D.H., Brain, D.A., Acuña, M.H., 2005. Low-frequency plasma oscillations at Mars during the October 2003 solar storm. J. Geophys. Res. 110, A09S33.

Fazakerley, A.N., Southwood, D.J., 1994. Mirror instability in the magnetosheath. Adv. Space Res. 14, 65–68.

Fitzenreiter, R.J., Burlaga, L.F., 1978. Structure of current sheets in magnetic holes at 1AU, NASA STI/Recon Technical Report N. 78, 20033.

Fränz, M. et al., 2006. Plasma moments in the environment of Mars. Mars Express ASPERA-3 observations. Space Sci. Rev. 126, 165–207.

Gekelman, W., Urrutia, J.M., Stenzel, R.L., 1987. Measurement of magnetic helicity during the disruption of a neutral current sheet. Magnetotail Physics, vol. 261. Johns Hopkins University Press.

Halekas, J.S., Brain, D.A., 2010. Global distribution, structure, and solar wind control of low altitude current sheets at Mars. Icarus 206, 64–73. http://dx.doi.org/10.1016/j.icarus.2008.12.032.

Halekas, J.S. et al., 2009. In situ observations of reconnection Hall magnetic fields at Mars: Evidence for ion diffusion region encounters. J. Geophys. Res. 114 (A13), 11204.

Halekas, J.S. et al., 2011. Large-amplitude compressive "sawtooth" magnetic field oscillations in the martian magnetosphere. J. Geophys. Res. 116, A07222. http://dx.doi.org/10.1029/2011JA016590.

Harnett, E.M., 2009. High-resolution multifluid simulations of flux ropes in the martian magnetosphere. J. Geophys. Res. 114, A01208. http://dx.doi.org/10.1029/2008JA013648.

Harnett, E.M., Winglee, R.M., 2003. The influence of a "mini-magnetopause" on the magnetic pileup boundary at Mars. Geophys. Res. Lett. 30, 2074. http://dx.doi.org/10.1029/2003GL017852.

Huang, C., Lu, Q., Lu, S., Wang, P., Wang, S., 2014. The effect of a guide field on the structures of magnetic islands formed during multiple X line reconnections: Two-dimensional particle-in-cell simulations. J. Geophys. Res. Space Phys. 119, 798–807. http://dx.doi.org/10.1002/2013JA019249.

Hubert, D., Harvey, C.C., Russell, C.T., 1989. Observations of magnetohydrodynamic modes in the Earth's magnetosheath at 0600 LT. J. Geophys. Res. 94, 17305–17309.

Kaufmann, R.L., Horng, J.T., Wolfe, A., 1970. Large amplitude hydromagnetic waves in the inner magnetosheath. J. Geophys. Res. 75, 4666.

Lillis, R.J., Fillingim, M.O., Brain, D.A., 2011. Three-dimensional structure of the martian nightside ionosphere: Predicted rates of impact ionization from Mars Global Surveyor magnetometer and electron reflectometer measurements of precipitating electrons. J. Geophys. Res. 116, 12317.

Lucek, E.A. et al., 1999. Identification of mirror mode structures in the Equator-S magnetic field data. Ann. Geophys. 17, 1560–1573.

Lundin, R. et al., 2006a. Plasma acceleration above martian magnetic anomalies. Science 311, 980–983.

Lundin, R. et al., 2006b. Auroral plasma acceleration above martian magnetic anomalies. Space Sci. Rev. 126, 333–354.

Ma, Y. et al., 2002. Three-dimensional multispecies MHD studies of the solar wind interaction with Mars in the presence of crustal fields. J. Geophys. Res. 107, 1282.

Mitchell, D.L. et al., 2001. Probing Mars' crustal magnetic field and ionosphere with the MGS electron reflectometer. J. Geophys. Res. 106 (E10), 23419–23428.

Morgan, D.D. et al., 2011. Dual-spacecraft observation of large-scale magnetic flux ropes in the martian ionosphere. J. Geophys. Res. 116 (A15), A02319.

Nielsen, E. et al., 2007. Local plasma processes and enhanced electron densities in the lower ionosphere in magnetic cusp regions on Mars. Planet. Space Sci. 55, 2164–2172.

Nykyri, K., Otto, A., Adamson, E., Tjulin, A., 2011. On the origin of fluctuations in the cusp diamagnetic cavity. J. Geophys. Res. 116, 6208–6220. http://dx.doi.org/10.1029/2010JA015888.

Nykyri, K., Otto, A., Adamson, E., Kronberg, E., Daly, P., 2012. On the origin of high-energy particles in the cusp diamagnetic cavity. J. Atmos. Sol-Terr. Phys. 87, 70–81.

Øieroset, M., Mitchell, D.L., Phan, T.D., Lin, R.P., Acuña, M.H., 2001. Hot diamagnetic cavities upstream of the martian bow shock. Geophys. Res. Lett. 28, 887–890.

Øieroset, M. et al., 2004. The magnetic field pile-up and density depletion in the martian magnetosheath: A comparison with the plasma depletion layer upstream of the Earth's magnetopause. Space Sci. Rev. 111, 33–114.

Priest, E.R., 1990. The equilibrium of magnetic flux ropes. Physics of magnetic flux ropes. Geophys. Monograph. 58, 1–22.

Riedler, W. et al., 1991. Interaction of the solar wind with the planet Mars – PHOBOS 2 magnetic field observations. Planet Space Sci. 39, 75–81.

Russell, C.T., Riedler, W., Schwingenschuh, K., Yeroshenko, Y., 1987. Mirror instability in the magnetosphere of Comet Halley. Geophys. Res. Lett. (6), , 644–64.

Russell, C.T., 1990. Magnetic flux ropes in the ionosphere of Venus. Physics of magnetic flux ropes. Geophys. Monograph. 58, 413–423.

Russell, C.T., Elphic, R.C., 1978. Initial ISEE magnetometer results: Magnetopause observations. Space Sci. Rev. 22, 681–715.

Russell, C.T., Elphic, R.C., 1979. Observations of magnetic flux ropes in the Venus ionosphere. Nature 279, 616–618.

Saunders, M.A., Russell, C.T., Sckopke, N., 1984. Flux transfer events – Scale size and interior structure. Geophys. Res. Lett. 11, 131.

Schwartz, S.J., Burgess, D., Moses, J.J., 1996. Low-frequency waves in the magnetosheath: Present status. Ann. Geophys. 14, 1134–1150.

Sheldon, R.B., Spence, H.E., Sullivan, J.D., Fritz, T.A., Chen, J., 1998. The discovery of trapped energetic electrons in the outer cusp. Geophys. Res. Lett. 25, 1825.

Slavin, J.A. et al., 2009. MESSENGER and Venus express observations of the solar wind interaction with Venus. Geophys. Res. Lett. 36, L09106. http://dx.doi.org/10.1029/2009GL037876.

Soobiah, Y.I.J. et al., 2013. Energy distribution asymmetry of electron precipitation signatures at Mars. Planet. Space Sci. 76, 10–27.

Sonnerup, B.U.Ö., Scheible, M., 1998. Minimum and maximum variance analysis. In: Paschmann, G., Daly, P.W. (Eds.), Analysis Methods for Multi-spacecraft Data. Int. Space Sci. Inst., Bern, pp. 185–220.

Stevens, M.L., Kasper, J.C., 2007. A scale-free analysis of magnetic holes at 1 AU. J. Geophys. Res. 112, A05109. http://dx.doi.org/10.1029/2006JA012116.

Tsurutani, B.T. et al., 1982. Lion roars and nonoscillator drift mirror waves in the magnetosheath. J. Geophys. Res. 87, 6060–6072.

Tsurutani, B.T., Southwood, D.J., Smith, E.J., Balogh, A., 1992. Nonlinear magnetosonic waves and mirror mode structures in the March 1991 Ulysses interplanetary event. Geophys. Res. Lett. (12), 1267–1270. http://dx.doi.org/10.1029/92GL00782.

Tsurutani, B.T., Southwood, D.J., Smith, E.J., Balogh, A., 1993. A survey of low frequency waves at Jupiter: The Ulysses encounter. J. Geophys. Res. 98, 21203–21216.

Turner, J.M., Burlaga, L.F., Ness, N.F., Lemaire, J.F., 1977. Magnetic holes in the solar wind. J. Geophys. Res. 82, 1921.

Uluşen, D., Brain, D.A., Mitchell, D.L., 2011. Observation of conical electron distributions over martian crustal magnetic fields. J. Geophys. Res. 116, 7214. http://dx.doi.org/10.1029/2010JA016217.

Vignes, D.M. et al., 2004. Magnetic flux ropes in the martian atmosphere: Global characteristics. Space Sci. Rev. 111 (1), 223–231.

Winningham, J.D., Frahm, R.A., Sharber, J.R., 2006. Electron oscillations in the induced martian magnetosphere. Icarus 182, 360–370.

Wong, H.K., Menietti, J.D., Lin, C.S., Burch, J.L., 1988. Generation of electron conical distributions by upper hybrid waves in the Earth's polar region. J. Geophys. Res. 93, 10025.

Yeroshenko, Y., Riedler, W., Schwingenschuh, K.I., Luhmann, J.G., Ong, M., Russell, C.T., 1990. The magnetotail of Mars: Phobos observations. Geophys. Res. Lett. 17, 885–888.

Zhang, T.L. et al., 2008a. Characteristic size and shape of the mirror mode structures in the solar wind at 0.72 AU. Geophys. Res. Lett. 35, 10106.

Zhang, T.L. et al., 2008b. Behavior of current sheets at directional magnetic discontinuities in the solar wind at 0.72 AU. Geophys. Res. Lett. 35, L24102. http://dx.doi.org/10.1029/2008GL036120.

Zhang, T.L. et al., 2012a. Magnetic reconnection in the near venusian magnetotail. Science 336, 567–570.

Zhang, T.L. et al., 2012b. Giant flux ropes observed in the magnetized ionosphere at Venus. Geophys. Res. Lett. 39, L23103. http://dx.doi.org/10.1029/2012GL054236.

Zou, H. et al., 2010. Effects of martian crustal magnetic field on its ionosphere. Sci. China, Technol. Sci. 53, 1717–1724.